GEOCHEMISTRY

# Ultrahigh-precision noble gas isotope analyses reveal pervasive subsurface fractionation in hydrothermal systems

**David V. Bekaert[1,2]*, Peter H. Barry[1], Michael W. Broadley[1,2], David J. Byrne[2], Bernard Marty[2], Carlos J. Ramírez[3], J. Maarten de Moor[4,5], Alejandro Rodriguez[4], Michael R. Hudak[1], Adam V. Subhas[1], Saemundur A. Halldórsson[6], Andri Stefánsson[6], Antonio Caracausi[7,8], Karen G. Lloyd[9], Donato Giovannelli[1,10,11,12], Alan M. Seltzer[1]**



**Mantle-derived noble gases in volcanic gases are powerful tracers of terrestrial volatile evolution, as they contain mixtures of both primordial (from Earth's accretion) and secondary (e.g., radiogenic) isotope signals that characterize the composition of deep Earth. However, volcanic gases emitted through subaerial hydrothermal systems also contain contributions from shallow reservoirs (groundwater, crust, atmosphere). Deconvolving deep and shallow source signals is critical for robust interpretations of mantle-derived signals. Here, we use a novel dynamic mass spectrometry technique to measure argon, krypton, and xenon isotopes in volcanic gas with ultrahigh precision. Data from Iceland, Germany, United States (Yellowstone, Salton Sea), Costa Rica, and Chile show that subsurface isotope fractionation within hydrothermal systems is a globally pervasive and previously unrecognized process causing substantial nonradiogenic Ar-Kr-Xe isotope variations. Quantitatively accounting for this process is vital for accurately interpreting mantle-derived volatile (e.g., noble gas and nitrogen) signals, with profound implications for our understanding of terrestrial volatile evolution.**

## INTRODUCTION

The unique distribution of volatiles (i.e., carbon, nitrogen, and water) at Earth's surface makes our planet habitable within the Solar System (*1*–*4*). Understanding how volatiles are distributed between terrestrial reservoirs (i.e., atmosphere, crust, mantle, and core) requires identification of primordial volatile signatures that have not been modified by shallow geologic processes. Determining the origin of terrestrial volatiles therefore requires the analysis of primordial volatiles that have been stored in the mantle for most of Earth's history. One promising means to characterize the geochemical composition of the deep Earth and inform the origin of primordial volatiles trapped in the mantle is to analyze deeply sourced mantle products (rocks, minerals, and gases) brought to Earth's surface via volcanism and tectonics. Although Earth's mantle represents the largest terrestrial reservoir for many volatiles [e.g., $H_2O$, C, N, and S; (*4*–*6*)], accurately determining the volatile element composition of the mantle by analyzing magmatic products is often challenging. The main reason for this is the ubiquitous overprinting of primordial volatiles by surface-derived components, during (i) storage at depth, where volatile-laden materials are pervasively returned to the mantle via subduction, (ii) emission at Earth's surface (and interaction with groundwater reservoirs), and potentially (iii) sampling, although a contribution from unfractionated air "contamination" during sample collection remains highly unlikely. Another major issue with tracing volatile elements at planetary scales is that most of these species are chemically reactive, meaning that their primordial compositions are likely to be affected by secondary processes (e.g., chemical partitioning and biological reactions) taking place within Earth's crustal reservoirs [e.g., (*7*)].

Noble gases are ideal tracers of planetary volatiles as they are chemically inert, highly volatile, and incompatible in melts (*8*). Given that noble gases are not affected by chemical or biological processes, their compositions within volcanic products are conventionally assumed to reflect a binary mixture between deep (mantle) and surficial (atmospheric, crustal, and sedimentary) components. Because the light isotopes of argon ($^{36,38}$Ar), krypton ($^{78,80,82}$Kr), and xenon ($^{124,126,128,130}$Xe) are not significantly produced by nuclear processes within the solid Earth, variations in their relative abundance ratios provide direct insight into the accretionary source(s) of terrestrial volatiles (*8*–*10*). Conversely, secondary noble gas isotopes have been produced by fissiogenic and radiogenic decay chains {e.g., $^{129}I \Rightarrow {}^{129}Xe$ [$T_{1/2}$ = 16 million years (Ma)], $^{244}Pu \Rightarrow {}^{131-136}Xe$ ($T_{1/2}$ = 80 Ma), $^{238}U \Rightarrow {}^{131-136}Xe$ [$T_{1/2}$ = 4.45 billion years (Ga)]} (*11*). Hence, they constitute key tracers of the timing and extent of mantle degassing to the atmosphere over geological time (*8*). Despite the great insight offered in principle by noble gases, the pervasive introduction of surface-derived Ar-Kr-Xe via subduction into the mantle over the past ~2 Ga has largely overprinted both primordial and secondary mantle signals (*12*, *13*), hence greatly complicating the interpretation of heavy noble signals in mantle-derived samples. Previous studies have shown that ~80% of the nonradiogenic Ar-Kr-Xe isotopes in the present-day mantle

[1]Marine Chemistry and Geochemistry Department, Woods Hole Oceanographic Institution, Woods Hole, MA 02543, USA. [2]Université de Lorraine, CNRS, CRPG, F-54000 Nancy, France. [3]Servicio Geológico Ambiental (SeGeoAm) Heredia, Santo Domingo, Costa Rica. [4]Observatorio Vulcanológico y Sismológico de Costa Rica Universidad Nacional, Heredia, Costa Rica. [5]Department of Earth and Planetary Sciences, University of New Mexico, Albuquerque, NM 87106, USA. [6]NordVulk, Institute of Earth Sciences, University of Iceland, Reykjavík, Iceland. [7]Instituto Nazionale di Geofisica e Vulcanologia, Sezione di Palermo, 90146 Palermo, Italy. [8]University of Salamanca, Salamanca, Spain. [9]Microbiology Department, University of Tennessee, Knoxville, TN 37996, USA. [10]Department of Biology, University of Naples Federico II, Naples, Italy. [11]Institute for Marine Biological and Biotechnological Resources, National Research Council of Italy, Ancona, Italy. [12]Department of Marine and Coastal Science, Rutgers University, New Brunswick, NJ 08901, USA.
*Corresponding author. Email: david.bekaert@univ-lorraine.fr

are derived from recycled atmospheric components (*12*, *14*). In addition, volcanic gases that are actively degassed from magma chambers can acquire atmosphere-derived noble gas components during their ascent through groundwater reservoirs and due to interaction with hydrothermal systems. Therefore, the fraction of mantle-derived heavy noble gases in volcanic gases worldwide is often minimal (below 1% of total heavy noble gas inventories), due to overprinting by both subduction/crustal assimilation and groundwater–volcanic gas interaction. In most cases, the magnitudes of mantle-derived Ar-Kr-Xe signals are thus comparable to (or lower than) the analytical precision of conventional static noble gas mass spectrometers, except for $^{40}Ar/^{36}Ar$. For decades, this analytical limitation has greatly hampered the widespread application of heavy noble gas isotope systematics in volcanic regions worldwide.

Despite these challenges, several studies have reported nonradiogenic Kr and Xe isotope anomalies [e.g., (*9*, *15*–*17*)], which have been interpreted to be carbonaceous meteorite-like in origin (*9*, *10*, *16*). Ne-Ar isotopes in volcanic gases may suggest pervasive physical fractionation processes in the subsurface before their emission at the surface [e.g., (*18*–*20*)]; however, no studies have investigated the possibility for volcanic heavy noble gas isotopes to be affected by similar physical fractionation processes. A recent study showed that isotope fractionation during sample preparation and/or analysis can lead to erroneous interpretations about the origin of volcanism and even mischaracterization of corresponding mantle reservoir compositions (e.g., the extent of mantle degassing to the atmosphere) (*17*), but the extent to which Ar-Kr-Xe isotope variations in volcanic systems can be interpreted as reflecting mantle source signals therefore remains unknown. These considerations require substantial improvements in the analytical precision and accuracy of heavy noble gas isotope measurements to confidently determine mantle source signals in volcanic gas measurements.

Noble gas analysis by dual-inlet dynamic mass spectrometry (DMS) has markedly improved analytical precision on volcanic noble gas measurements (*21*). With a dynamic mass spectrometer, often called an "isotope ratio mass spectrometer," the rapid switching between analysis of sample and reference gas streams reduces the effect of instrumental drift (*22*) and thus greatly enhances analytical precision (on the order of ~0.01‰). In addition, a suite of robust corrections and the capacity to measure air and air-equilibrated water (AEW) samples in an identical manner to volcanic gases (*21*), against the same reference gas, increases the overall accuracy compared to traditional, static mass spectrometry methods (≥1‰). In this study, we present Ar-Kr-Xe isotopes from natural $CO_2$-rich gases collected in Iceland, Germany, United States, Costa Rica, and Chile, measured by DMS, following recent analytical developments in the Seltzer Lab at Woods Hole Oceanographic Institution (WHOI) (*21*). The ultrahigh precision and accuracy of these volcanic noble gas measurements reveal that physical isotope fractionation processes in the subsurface ubiquitously generate variable enrichments in the light Ar, Kr, and Xe isotopes in volcanic gases. The magnitude of the largest observed Ar-Kr-Xe isotopic deviations from the atmosphere exceeds the kinetic fractionation factors associated with diffusion in water (*23*–*25*), implying that isotopic fractionation (up to several ‰) primarily arises from gas-phase diffusion of noble gases that presumably degas from groundwater and diffuse through $CO_2$ in the subsurface (*20*, *26*). We show that subsurface fractionation processes represent a widespread and critical phenomenon that need to be quantitatively assessed before interpreting volatile isotope variations in volcanic gas from hydrothermal systems. Using empirical relationships between Ar-Kr-Xe abundances and isotopic ratios, we demonstrate that measured noble gas compositions can be robustly corrected for physical fractionation effects, hence opening the door to resolving mantle signals in orders of magnitude more volcanic samples worldwide than previously possible, at a greater precision and accuracy than achieved to date. In addition to high-precision noble gas measurements by DMS, we report the C isotope composition of Giggenbach solutions (i.e., $CO_2$-saturated sodium hydroxide), measured using a Picarro G-2131i cavity ringdown spectrometer connected to an AutoMate-Liaison prep device in the Subhas Lab at WHOI. We also report the nitrogen and helium isotope composition of volcanic gas samples collected with copper tubes along with Giggenbach samples and measured in the Barry Lab at WHOI.

## RESULTS

Results are reported in per mil (‰) using delta notation, where a given isotopic or elemental ratio (noted $R$) is expressed as $\delta R = \left(R_{sample}/R_{atmosphere} - 1\right) \times 1000$. We achieve an analytical precision on the order of 0.01 to 0.1‰ for all Ar, Kr, and Xe isotope ratios (Fig. 1; data are reported in the Supplementary Materials), which is one to two orders of magnitude better than previously achieved with conventional techniques.

In volcanic gases, $\delta^{40}Ar/^{36}Ar$ represents a useful tracer of non-atmospheric sources of heavy noble gases, since both mantle and crustal sources are enriched in $^{40}Ar$ relative to the atmosphere ($^{40}Ar/^{36}Ar_{ATM}$ = 298.6) due to the radioactive decay of $^{40}K$ ($T_{1/2}$ = 1.251 Ga). The $\delta^{40}Ar/^{36}Ar$ values reported in this study vary from −7‰ (Iceland, $^{40}Ar/^{36}Ar$ = 296.5) to 3482‰ (i.e., $^{40}Ar/^{36}Ar$ = 1338.3) in Eifel (Germany) (fig. S1). The large range in observed $\delta^{40}Ar/^{36}Ar$ primarily reflects varying contributions from deep (mantle or crustal) versus atmospheric sources of heavy noble gases. Across our entire sample set ($n$ = 30 samples; from Europe, North America, South America, and Central America), we observe that nonradiogenic Ar, Kr, and Xe isotope ratios exhibit highly correlated light isotope enrichments relative to the atmosphere (Fig. 1). The magnitudes of these isotopic variations are on the order of several per mil, which is comparable to those of volcanic gas isotope deviations from the atmospheric composition that have previously been interpreted as deep, mantle signals [e.g., (*9*, *16*, *17*)].

Noble gas elemental ratios in volcanic gases broadly span the entire range between unfractionated air (i.e., $\delta^{84}Kr/^{36}Ar$ and $\delta^{130}Xe/^{36}Ar$ ~ 0‰) and AEW (Fig. 2A). Several samples (e.g., from the Chilean volcanic arc) have $\delta^{84}Kr/^{36}Ar$ and $\delta^{130}Xe/^{36}Ar$ values that plot above the AEW range, suggesting potential contributions from Kr- and Xe-rich components possibly associated with subducted organic and sedimentary material (*12*). Most volcanic gases also show small, but significant, deviations from an air-AEW mixing line toward higher $\delta^{132}Xe/^{36}Ar$ values (Fig. 2A). Last, we note that significant nonradiogenic heavy noble gas isotope fractionation (i.e., light isotope enrichments) seems to only occur in samples with intermediate Kr/Ar and Xe/Ar ratios between air and AEW (Fig. 2B).

Most of the $\delta^{13}C$ of $CO_2$ trapped in Giggenbach NaOH solutions (from Yellowstone, Iceland, Eifel, Cost Rica, and Salton Sea) show values intermediate between pure mantle ($\delta^{13}C$ ~ −5‰) and

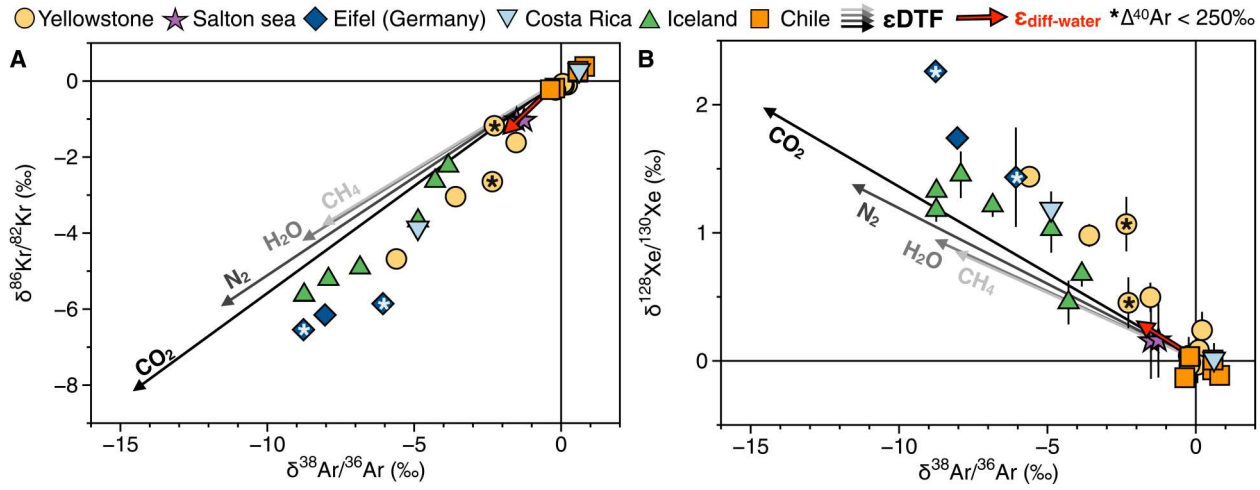


**Fig. 1. Nonradiogenic Ar-Kr-Xe isotope variations across all volcanic noble gas samples analyzed in this study, reported using delta notation relative to the atmosphere.** (**A** and **B**) Predictions for steady-state isotope fractionation via diffusive transport fractionation (DTF) through $CH_4$, $H_2O$, $N_2$, and $CO_2$ are given as vectors. Samples with $\Delta^{40}Ar = \delta^{40}Ar/^{36}Ar - 2*\delta^{38}Ar/^{36}Ar > 250‰$ (i.e., $^{40}Ar/^{36}Ar \geq 373$, if $\delta^{38}Ar/^{36}Ar = 0‰$) are noted with asterisks.

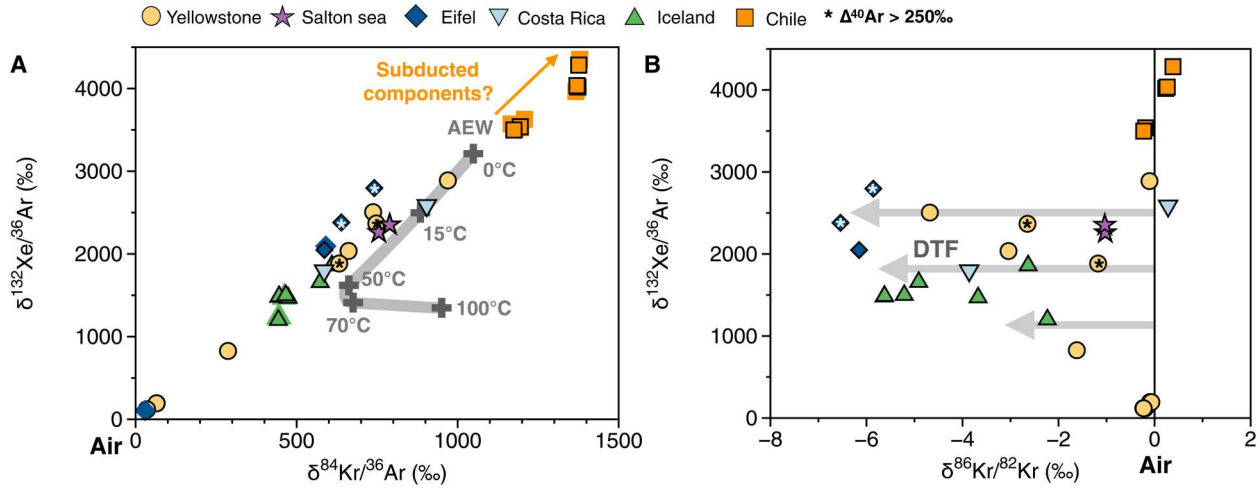


**Fig. 2. $\delta^{132}Xe/^{36}Ar$ versus $\delta^{84}Kr/^{36}Ar$ composition of all volcanic noble gas samples analyzed in this study, reported using the delta notation relative to the atmospheric isotope composition.** (**A**) The heavy noble gas composition of AEW (*56*) is given for comparison, as a function of temperature (from 0° to 100°C). Symbols with and without black outlines have been analyzed by DMS on MAT253$^+$ and MAT253 (both instruments in Seltzer Lab, WHOI), respectively. (A) and (**B**) Samples with $\Delta^{40}Ar > 250‰$ (i.e., $^{40}Ar/^{36}Ar \geq 373$, if $\delta^{38}Ar/^{36}Ar = 0‰$) are noted with asterisks.

carbonate ($\delta^{13}C \sim 0‰$) end-members (fig. S2) (*7*). Only Chilean arc samples show $\delta^{13}C$ values of <−5‰, in the range of −8.6 to −11.4‰. This result is consistent with independent $\delta^{13}C$ data acquired from gas vials that were collected along with the Giggenbach bottles analyzed in this study [$\delta^{13}CO_2$ = −8.72 and −8.64‰ for Campanario and Baño Morales, respectively (*27*)]. $\delta^{15}N$ values vary from −9.24‰ (Forrest Spring) to 0.13‰ (Crater Hills) for Yellowstone, from −3.32 to −0.86‰ for Iceland (Krýsuvík), and from −1.94‰ (Baño Morales) to 4.17‰ (Campanario) for Chile (typical uncertainty of ±0.8‰; fig. S3).

## DISCUSSION

This ultrahigh precision of DMS measurements offers the unique opportunity to constrain the heavy noble gas (Ar-Kr-Xe) isotope composition of mantle sources and identify potential processes that may affect mantle isotope compositions before their emission at Earth's surface. Here, the observation of negative $\delta^{40}Ar/^{36}Ar$ values cannot be ascribed to any source effect, as all geological reservoirs within the solid Earth are enriched in radiogenic $^{40}Ar$ relative to the atmospheric composition due to $^{40}K$ decay. Rather, a negative $\delta^{40}Ar/^{36}Ar$ value must indicate a physical fractionation process that induces enrichment in the light isotopes of Ar. In such an instance, $\delta^{38}Ar/^{36}Ar$ may be used to correct $\delta^{40}Ar/^{36}Ar$ for physical fractionation [e.g., (*28*, *29*)] by considering that (i) $\delta^{40}Ar/^{36}Ar$ is fractionated by mass-dependent processes by twice the magnitude of $\delta^{38}Ar/^{36}Ar$ fractionation, and (ii) the initial source $\delta^{38}Ar/^{36}Ar$ is zero, as there are no significant sources of $^{38}Ar$ or $^{36}Ar$ within the solid Earth. Nonradiogenic Ar-Kr-Xe isotope variations reported in this study are not correlated with

$\delta^{40}Ar/^{36}Ar$ (fig. S1). For example, Icelandic samples span a large range of nonradiogenic Ar-Kr-Xe isotope variations (Fig. 1) despite having only marginal $^{40}Ar$ excesses from a deep noble gas contribution ($\delta^{40}Ar/^{36}Ar \leq 14‰$ for all Icelandic samples analyzed in this study). Therefore, the consistent patterns of isotopic and elemental fractionation of heavy noble gases across vastly different volcanic gas systems around the world do not reflect a deep source contribution. They rather point to previously unrecognized mechanism (or series of mechanisms) of physical fractionation, which appears to be ubiquitous in the subsurface of volcanic systems. Understanding the origin of these isotope signals and their correlations across noble gases is critical for assessing whether prior studies have incorrectly interpreted physical fractionation signals as mantle source signals.

Here, we make use of the global consistency in nonradiogenic isotope fractionation and present an empirical approach by which Kr isotopes can be used to robustly correct Xe isotopes for fractionation in the subsurface. We show that this method successfully resolves radiogenic and fissiogenic Xe isotope anomalies, even in samples that have been markedly affected by subsurface fractionation. The combination of our new DMS technique (*21*) and correction approach allows for the detection of crustal and mantle Xe isotope anomalies at the sub-1‰ level, providing unprecedented insight into deeply sourced Xe isotope signals. Using these data, we construct a model to explain subsurface fractionation mechanisms. The model broadly reproduces the observed isotopic and elemental fractionation patterns, thus validating our approach.

## Physical constraints on diffusive transport fractionation

What is the dominant process (or series of processes) causing the observed consistent fractionation of nonradiogenic Ar, Kr, and Xe isotope ratios in volcanic gases? A central clue is that the magnitude of most Ar-Kr-Xe isotopic deviations from the atmosphere exceeds the kinetic fractionation factors due to diffusion in water (*23*–*25*) (Fig. 1), implying that large isotopic fractionation (on the order of several per mil) must primarily arise from gas-phase diffusion of noble gases. A second clue is that the only significant nonradiogenic heavy noble gas isotope fractionation occurs in samples with intermediate Kr/Ar and Xe/Ar ratios between air and AEW (Fig. 2B). This observation rules out sampling artifacts (e.g., air leakage) as the source of isotopic fractionation, as leakage would induce Kr/Ar and Xe/Ar ratios below air, with extensive kinetic fractionation favoring the light isotope. Instead, this gas-phase fractionation must occur in the subsurface, presumably due to diffusion of degassed groundwater-derived noble gases against $CO_2$. The magnitude and direction of nonradiogenic Ar-Kr-Xe isotope variations appear compatible with the known steady-state fractionation factors for diffusive transport fractionation (DTF) of noble gas isotopes against $CO_2$ (Fig. 1) (*20*, *26*). If groundwater-derived noble gases degas into a $CO_2$ gas phase in the deep subsurface (e.g., via $CO_2$ stripping) and then diffuse through the $CO_2$ gas phase toward the center of the upwelling plume, then the difference between the diffusion coefficients of heavy (slow) and light (fast) isotopes will produce a steady-state depletion of the heavy isotopes (Fig. 3C) (*20*). Fractionation factors can be computed from the ratios of binary diffusion coefficients for two gas pairs (molecules or isotopes) (*30*, *31*). For example, the ratio $R_k(i/j)$ of the binary diffusion coefficients of two isotopes $i$ and $j$ (e.g., $^{128}Xe$ and $^{130}Xe$) diffusing through a gaseous medium $k$ (e.g., $CO_2$) can be computed as

$$R_k\left(\frac{i}{j}\right) = \sqrt{\frac{[m(i)+m(k)]\times[m(j)\times m(k)]}{[m(j)+m(k)]\times[m(i)\times m(k)]}} \times \left[\frac{V(j)^{1/3}+V(k)^{1/3}}{V(i)^{1/3}+V(k)^{1/3}}\right]^2 \quad (1)$$

where $m$ refers to the mass of each molecule or isotope, and $V$ refers to their dimensionless diffusion volumes [$V(N_2)$ = 18.5, $V$(Ar) = 16.2, $V$(Kr) = 24.5, $V$(Xe) = 32.7, $V(CO_2)$ = 26.9, $V(H_2O)$ = 13.1, $V(CH_4)$ = 25.4; determined by regression analysis of experimental gas-phase diffusivities (*31*, *32*)]. Hence, the magnitude of DTF directly depends on the atomic mass of the gas in the medium (Fig. 1) (*20*). In the case of $CO_2$, steady-state isotope fractionation of Ar, Kr, and Xe isotopes yields ~7, 2, and 1‰ per mass unit ($u^{-1}$), respectively (i.e., about −14‰ for $\delta^{38}Ar/^{36}Ar$, −8‰ for $\delta^{86}Kr/^{82}Kr$, and +2‰ for $\delta^{128}Xe/^{130}Xe$; Fig. 1). For most volcanic sites, the observed ranges of $\delta^{38}Ar/^{36}Ar$, $\delta^{82}Kr/^{84}Kr$, $\delta^{86}Kr/^{84}Kr$, and $\delta^{128}Xe/^{130}Xe$ are compatible with variable extents of DTF against $CO_2$, starting from an isotopically AEW-like [effectively, air-like; (*25*)] gas phase. It is nonetheless noteworthy that the slopes of the Kr-Ar (Fig. 1A) and Xe-Ar (Fig. 1B) isotopic trends do not exactly follow predictions from steady-state isotope fractionation via diffusive transport through $CO_2$, pointing to greater extents of Xe and Kr isotope fractionation relative to Ar. Given that Ar diffusion in water is faster than for the heavier noble gases, it more readily reaches isotopic equilibrium with the $CO_2$ gas phase, thereby limiting the effect of kinetic isotope fractionation. Conversely, Xe and Kr diffuse more slowly than Ar, implying that they are more prone to kinetic isotope fractionation (fig. S4).

## Empirical correction of Xe isotopes for DTF

Quantifying and ultimately correcting for, physical fractionation is crucial to robustly interpret mantle and crustal heavy noble gas signals as tracers of terrestrial volatiles. To this end, we only consider samples for which heavy noble gases are clearly dominated by an atmospheric source (that is, $\Delta^{40}Ar = \delta^{40}Ar/^{36}Ar - 2^{*}\delta^{38}Ar/^{36}Ar$ < 250‰, or $^{40}Ar/^{36}Ar$ < 373 if $\delta^{38}Ar/^{36}Ar$ = 0‰), such that crustal and mantle-derived heavy noble gas fractions are minimal (i.e., less than 1%). When reported relative to $\delta^{86}Kr/^{84}Kr$ (the same observation would be valid for $\delta^{82}Kr/^{84}Kr$; figs. S5 and S6), $\delta^{128}Xe/^{130}Xe$ values define a strong linear correlation with a slope of −0.5331 ± 0.0179 [95% confidence interval (CI); Fig. 4].

This strong correlation provides a robust empirical means for using Kr isotopes as a tracer of the extent of DTF to correct each Xe isotope spectrum for physical fractionation in the subsurface. In detail, the extent to which each $\delta^{128}Xe/^{130}Xe$ should be corrected for the effect of DTF is computed as

$$\delta^{128}Xe/^{130}Xe_{DTF-corr} = (-0.5331 \pm 0.0179) \times \delta^{86}Kr/^{84}Kr \quad (2)$$

The extent of DTF correction is then propagated to the rest of the Xe isotope ratios following

$$\delta^{i}Xe/^{130}Xe_{DTF-corr} = \frac{\delta^{128}Xe/^{130}Xe_{DTF-corr} \times \{[R_{CO_2}\left(\frac{^{i}Xe}{^{130}Xe}\right) - 1] \times 1000\}}{[R_{CO_2}\left(\frac{^{128}Xe}{^{130}Xe}\right) - 1] \times 1000} \quad (3)$$

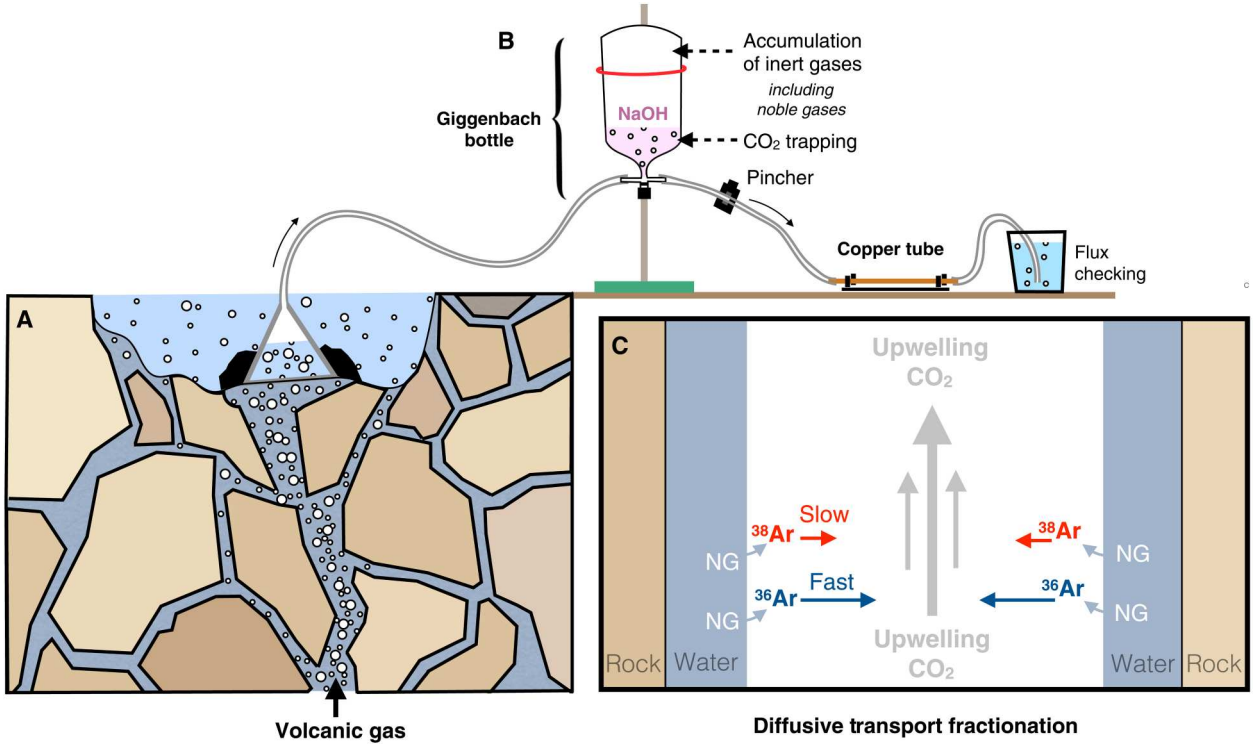


**Fig. 3. Schematic representation of typical volcanic gas collection and illustration of DTF.** (**A** to **C**) Cross-section of the subsurface, where volcanic gas (mainly $CO_2$) ascends through shallow groundwater until it reaches the surface. Part of the gas is captured by an upside-down funnel submerged in surficial water. The captured gas then flows through the tubing system and copper tube, until it reaches the preevacuated Giggenbach bottle containing a 5 N NaOH solution (*17*, *51*). Because of the pressure gradient across the NaOH solution, a fraction of the volcanic gas is sucked into the Giggenbach bottle, where $CO_2$ dissolves in solution and inert gases accumulate in the headspace. $CO_2$ bubble stripping of groundwater-derived noble gases is a ubiquitous process that accounts for the occurrence of air-derived components with AEW elemental abundances in volcanic gas systems (Fig. 2) (*45*). Groundwater-derived noble gases then experience diffusive transport against $CO_2$ [also referred to as "binary" or "mutual" diffusion; (*20*, *26*)]. The difference between the diffusion coefficients of heavy (slow) and light (fast) isotopes (here, only $^{36}Ar$ and $^{38}Ar$ are shown for illustrative purpose) produces a depletion of the heavy isotopes (in this case, $^{38}Ar$), whose magnitude depends on the atomic mass of the gas in medium (*20*).

This correction is fundamental for providing unbiased access to deep Xe isotope signals originating from mantle and crustal sources. Combining DMS measurements with the use of Kr isotopes as proxies of DTF to correct Xe isotopes for physical fractionation enables quantification of mantle-derived Xe isotope signals that were previously inaccessible.

## DMS to unravel crustal and mantle-derived noble gas signals

To illustrate the potential of DMS and the quantitative insight offered by the DTF correction (namely, the use of ultrahigh-precision Kr isotope ratio measurements to correct for mass-dependent fractionation of Xe isotopes), we present two case studies: Yellowstone National Park and Eifel volcanic province. Volcanic gas samples were collected along a north-south transect from the edge of the Yellowstone caldera (Washburn spring) to its center (Mud Volcano) (Fig. 5). While He isotopes lower than air ($^3He/^4He \sim 0.6$ times the atmospheric ratio, $R_A$; Supplementary Materials) indicate a major influence of crustal components in Washburn spring, He isotopes measured at Mud Volcano exhibit the highest values ever reported across the park [(*33*); here, $R_c/R_A = 19.49 \pm 0.19$, with $R_c$ corresponding to the measured $^3He/^4He$ corrected for the presence of atmospheric He]. Helium isotope systematics therefore point to an increasing contribution of pristine Yellowstone mantle plume gas toward the center of the caldera [e.g., (*33*)]. Here, Washburn spring volcanic gas shows clear fissiogenic Xe isotope excesses (noted $\delta^{131-136}Xe^*$) that, after correction for DTF (Supplementary Materials), are not associated with any excess of mantle-derived $^{129}Xe$ (noted $\delta^{129}Xe^*$) (Fig. 5A). Such a decoupling implies that fissiogenic Xe isotope excesses at Washburn spring must primarily arise from U decay within the continental crust, in line with independent evidence for significant crustal He contribution (*33*). Moving away from the edge of the caldera, $\delta^{131-136}Xe^*$ and $\delta^{129}Xe^*$ increase with distance, in line with a rising contribution of pristine Yellowstone mantle plume gas (Fig. 5F). Here, we define $F_{CM}$ as the ratio $(\delta^{136}Xe^* - \delta^{129}Xe^*)/\delta^{136}Xe^*$, which provides an indication as to whether fissiogenic Xe isotope excesses are predominantly from crustal or mantle source. If $F_{CM} \sim 1$, then most (if not all) of $^{136}Xe^*$ is of crustal origin, whereas if $F_{CM} \sim 0$ [i.e., if the magnitudes of $\delta^{136}Xe^*$ and $\delta^{129}Xe^*$ are similar, which is typical for mantle Xe (*17*)], then most (if not all) of $\delta^{136}Xe^*$ is of mantle origin (*9*). Here, we observe a clear evolution from $F_{CM} \sim 1$ at Washburn spring toward $F_{CM} \sim 0$ at Mud Volcano (Fig. 5D), clearly pointing to a decreasing contribution of the crustal component and an increasing contribution of the mantle component toward the center of the caldera (in line with He isotope systematics; fig. S7). The large discrepancies between raw data and those corrected for DTF highlights the need to apply

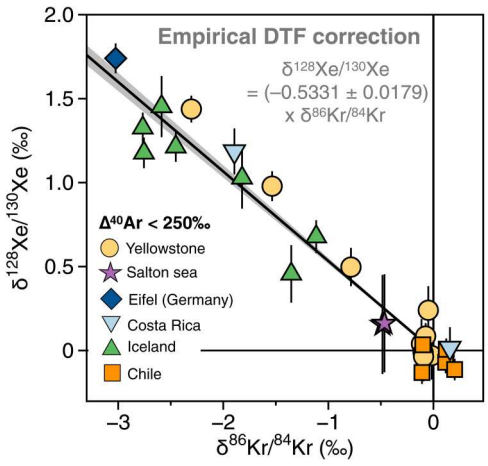


**Fig. 4. Empirical relationship between $\delta^{128}Xe/^{130}Xe$ and $\delta^{86}Kr/^{84}Kr$, used to correct Xe isotopes for DTF.** The slope of the regression (−0.5331 ± 0.0179; 95% CI, Mean Squared Weighted Deviation (MSWD) = 1.78) is obtained by using the error weighted least squares algorithm of (*59*), forcing the regression through the origin. This correction is required to yield unbiased access to deep Xe isotope signals originating from mantle and crustal sources. Note that the same approach can be used by using $\delta^{82}Kr/^{84}Kr$ instead of $\delta^{86}Kr/^{84}Kr$ (fig. S5).

robust DTF corrections before interpreting heavy noble gas data from volcanic emissions in Yellowstone National Park.

The second case study focuses on noble gas measurements from Eifel (in Heckenmünster, Germany), where volcanic gases originate from the upper mantle (*17*). We sampled two distinct locations [Victoriaquelle (E-VQ) and Schwefelquelle (E-SQ)], which are only separated from one another by ~150 m. The E-VQ sample from Eifel has the highest $\delta^{40}Ar/^{36}Ar$ (= 3482‰, i.e., $^{40}Ar/^{36}Ar$ = 1338) reported in this study, indicating significant (i.e., several %-level) contribution of pure upper mantle gas. The E-SQ has a much lower $\delta^{40}Ar/^{36}Ar$ (= 149‰, i.e., $^{40}Ar/^{36}Ar$ = 343), indicating minimal upper mantle contributions. Nonetheless, both samples exhibit comparable enrichments in the light Xe isotopes ($\delta^{128}Xe/^{130}Xe$ ~ 1.5‰) arising from DTF (Fig. 6A). Despite the elevated $\delta^{40}Ar/^{36}Ar$ of E-VQ, the DTF correction markedly affects the relative excesses of mantle-derived Xe signals (Fig. 6), which further demonstrates the need to robustly correct measured Xe isotope spectra for physical fractionation before interpreting mantle-derived Xe isotope excesses. When comparing the E-VQ and E-SQ Xe isotopic spectra by normalizing E-SQ to the $\delta^{129}Xe^*$ of E-VQ after correction for DTF (Fig. 6), we observe excellent agreement between the two Xe isotope spectra (within uncertainty), which further validates the DTF correction. When MV1 (Yellowstone) is normalized to the $\delta^{129}Xe^*$ of E-VQ after correction for DTF, it exhibits a $\delta^{136}Xe^*$ that is slightly higher than—but still similar to—E-VQ (Fig. 6). This suggests a comparatively greater contribution from crustal, U-derived Xe at Mud Volcano. Alternatively, this discrepancy could reflect a pristine mantle source heterogeneity, with a greater $^{129}Xe$ excess in the mantle source of Eifel gas (i.e., upper mantle) than that in the deep mantle source of the Yellowstone plume (*8*, *17*). Although beyond the scope of this small case study, one promising avenue to distinguish between those two possibilities, enabled by the advances in the present work, is to deconvolve fissiogenic Xe isotope excesses into uranium- and plutonium-derived sources.

Because $^{244}Pu$ became extinct ~4 Ga ago and $^{238}U$ is still extant, mantle reservoirs that underwent extensive degassing over geological time have lost a significant fraction of Pu-produced fission Xe ($^{136}Xe_{Pu}$), which originally represented ~97% of the total fissiogenic Xe. As a result, extensively degassed mantle reservoirs present a large proportion of $^{238}U$-derived fission Xe ($Xe_U$) (*11*). The deconvolution of $^{136}Xe_{Pu}$ and $^{136}Xe_U$ contributions in volcanic gases thus enables an estimation of the fraction of fissiogenic $^{136}Xe$ that is derived from $^{136}Xe_{Pu}$, which illustrates the heterogeneous nature of Earth's degassing. Variations in Xe isotopes have been used to suggest that the upper mantle source (i) experienced catastrophic degassing within the first 100 Ma of planetary evolution (*34*) and (ii) has remained isolated from the more primitive lower mantle for most of Earth's history (*35*). Our new Xe isotope data indicate a clear potential for DTF to markedly affect the relative ratios of Xe isotope excesses in volcanic gases, thereby skewing the deconvolution and interpretation of fissiogenic Xe isotope excesses.

Here, we only consider Yellowstone and Eifel samples with the highest mantle contributions reported in this study (i.e., MV1 and E-VQ, respectively). In $^{132}Xe^*/^{136}Xe^*$ versus $^{134}Xe^*/^{136}Xe^*$ space, where $^iXe^*$ refers to the fissiogenic excess of isotope $^iXe$ relative to the atmospheric composition and to the $^{130}Xe$ abundance, uncorrected volcanic noble gas data plot away from the expected array between Pu- and U-derived Xe end-members (Fig. 7). Once corrected for DTF, the E-VQ sample from Eifel plots in agreement with the pure U-derived Xe end-member (Fig. 7), which is in line with previous findings from Xe isotope analysis by static mass spectrometry of a very pristine Eifel gas sample with a $^{40}Ar/^{36}Ar$ ~8300 [i.e., ~30% pure mantle Xe contribution (*17*)]. This result demonstrates that, following correction for DTF, Xe isotope measurements by DMS, of a volcanic gas with only ~3% mantle Xe contribution (e.g., E-VQ), can be used to sufficiently determine whether the mantle source reservoir is dominated by Pu- or U-derived fissiogenic Xe. For the Yellowstone samples, the MV1 sample also appears most compatible with a U-dominated signature of fissiogenic Xe (Fig. 7). This result is, however, unexpected, as mantle plumes like Yellowstone are considered to tap into deep, relatively undegassed portions of the mantle and should therefore retain a greater proportion of Pu-Xe than U-Xe (*9*, *36*). Although Pu-Xe dominated signatures have previously been reported in samples from the Icelandic and Samoan plumes (*36*), whether this feature also applies to the Yellowstone plume mantle remains to be seen. Additional high-precision DMS analyses of Yellowstone volcanic gases are required to further quantify fissiogenic Xe isotope contributions to the Yellowstone mantle source and establish the degassing history of the corresponding reservoir.

## Implications of DTF for other volatile species in volcanic systems

The physical processes of DTF, clearly identified in this study from ultrahigh-precision noble gas data, could affect a variety of other elements that are used to understand the origin and evolution of mantle volatiles. For instance, isotopic constraints on the nitrogen composition of both surface (e.g., atmosphere and slabs) and mantle reservoirs have long been used to explore the secular evolution of volatile cycling between Earth's surface and interior (*4*). Although recently called into question (*37*), the heavy $\delta^{15}N$ of deep mantle reservoirs (about +3‰) and light $\delta^{15}N$ of the upper mantle (about −5‰) relative to the atmosphere have been

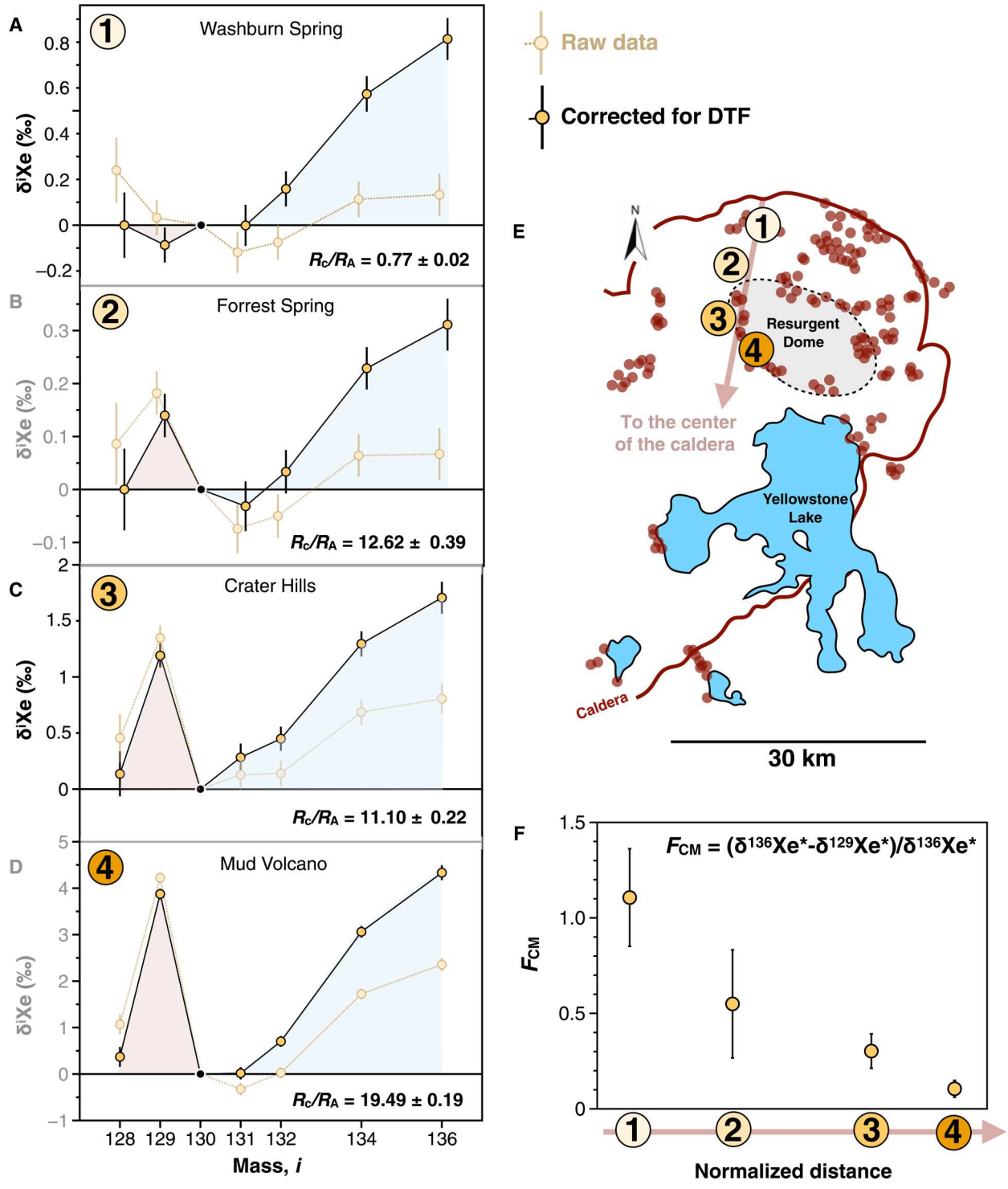


**Fig. 5. Overview of Xe isotope systematics across Yellowstone National Park.** (**A** to **F**) Xe isotopic spectra of volcanic gas samples collected along the north-south transect from the edge of the Yellowstone caldera (Washburn spring) to its center (Mud Volcano). For each sample, the raw data and data corrected for DTF (Fig. 4 and fig. S6) are both displayed for comparison. Helium isotope compositions are given for (*33*). The schematic map of Yellowstone National Park shows the location of the four sampling sites analyzed in this study. Thermal areas across the Yellowstone National Park are shown as red circles. The evolution of the $F_{CM}$ parameter [= ($\delta^{136}Xe^* - \delta^{129}Xe^*)/\delta^{136}Xe^*$] across the four samples analyzed in this study, as a function of the distance along the north-south transect from Washburn spring to Mud Volcano, demonstrates a clear evolution from a primarily crustal ($F \sim 1$) to a primarily mantle-sourced ($F \sim 0$) volcanic setting. Helium isotope data measured in the Barry Lab are reported for each sample (Supplementary Materials).

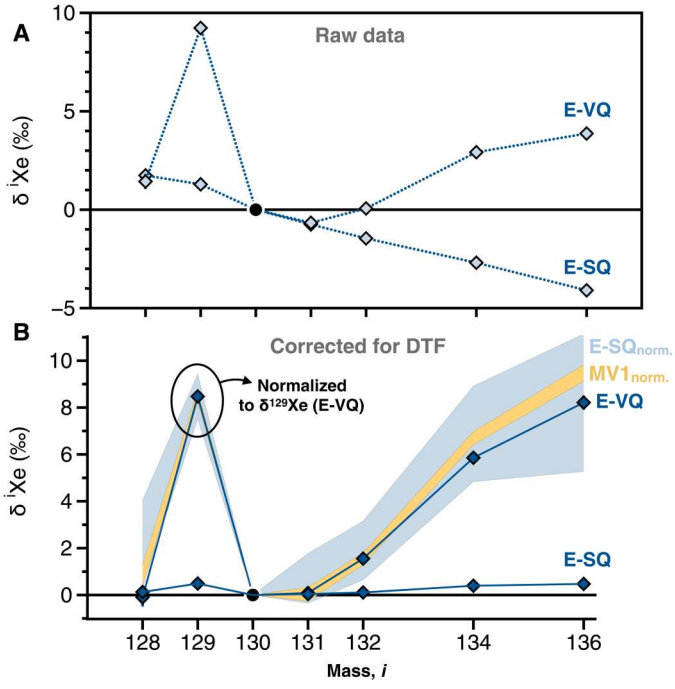


**Fig. 6. Xe isotopic spectra of volcanic gas samples collected in Eifel (Germany).** (**A** and **B**) The two samples collected at E-VQ and E-SQ show similar extents of DTF (e.g., comparable $\delta^{128}Xe/^{130}Xe$) but distinct radiogenic and fissiogenic isotope excesses. Whether variations in mantle gas contributions from one site to the other, and from one sampling campaign to the other, primarily reflect changes in volcanic activity or climatic parameters remains unclear. After correction for DTF, the Xe isotope composition of E-VQ (Eifel) and MV1 (Yellowstone) is compared to one another by normalizing the MV1 spectrum (Fig. 5D) to the $^{129}Xe$ excess of E-VQ. The brown shaded area shows the uncertainty envelope of the $^{129}Xe$-normalized MV1 spectrum. Slightly higher excesses in fissiogenic Xe isotopes in MV1 compared to E-VQ could potentially arise from the greater $^{129}Xe$ excess in the upper mantle (source of Eifel gas) compared to deep mantle (source of the Yellowstone plume) (*8*, *17*).

interpreted as reflecting the progressive addition of subducted sedimentary material ($\delta^{15}N$ about +6‰) to an initially $^{15}N$-depleted mantle (*4*, *38*, *39*). Over the past four decades, geochemical analyses of volcanic gases in hydrothermal systems have revealed a large range of $\delta^{15}N$, from −10.5 to +3.0‰ [e.g., (*40*)]. These variations have been tentatively attributed to either (i) kinetic fractionation of atmospheric nitrogen, (ii) occurrence of a light, mantle-derived nitrogen component [e.g., (*40*, *41*)], or (iii) stable isotope fractionation related to N devolatilization and decomposition (*42*). Recently, a new isotopologue approach was developed (*37*) to disentangle the contributions of air and mantle $N_2$ from the analysis of $^{15}N^{15}N$ abundances in volcanic $N_2$ gas. These $^{15}N^{15}N$ abundances can be compared to a random distribution of $^{14}N$ and $^{15}N$ atoms among $N_2$ molecules [$\Delta^{30}N = {}^{30}R/({}^{15}R)^2 - 1$ (‰), where $^{30}R = {}^{15}N^{15}N/{}^{14}N^{14}N$ and $^{15}R = {}^{15}N/{}^{14}N$] to unambiguously distinguish high-temperature (i.e., mantle-derived) sources of $N_2$ (with $\Delta^{30}N \sim 0$) from atmosphere-derived components ($\Delta^{30}N \sim 19$‰) (*37*). The authors observed that Iceland and Yellowstone volcanic gas samples displayed $\delta^{15}N$ variations between approximately −10 and 0‰, despite exhibiting atmosphere-like $\Delta^{30}N$ values, indicating that some unknown process must be causing significant fractionation of air-derived nitrogen in volcanic systems (*37*, *43*). On the basis of Eq. 1, we compute that steady-state DTF of $N_2$ corresponds to a $\delta^{15}N$ of −10.6‰, fully consistent with the range of $\delta^{15}N$ values observed for volcanic gas samples worldwide (*40*, *41*), including those with atmospheric $\Delta^{30}N$ (*37*). Consistent with noble gas systematics (Fig. 2B), $\delta^{15}N$ data with atmospheric $\Delta^{30}N$ values (*37*) inversely correlate with $\delta^{84}Kr/^{36}Ar$ and $\delta^{132}Xe/^{36}Ar$ ratios (Fig. 8): The most fractionated samples fall within the $\delta^{84}Kr/^{36}Ar$ range that is intermediate between air ($\delta^{84}Kr/^{36}Ar = 0$‰) and AEW ($\delta^{84}Kr/^{36}Ar \sim 800$‰) values, with the least fractionated samples showing ASW-like $\delta^{84}Kr/^{36}Ar$ (Fig. 8). This is opposite to any prediction based on the respective solubilities of these gases under ideal conditions (*37*, *44*), but consistent with observations for DTF as reported in this study (Fig. 2B), indicating that DTF is (one of) the primary cause(s) of $\delta^{15}N$ variations in volcanic systems (*43*).

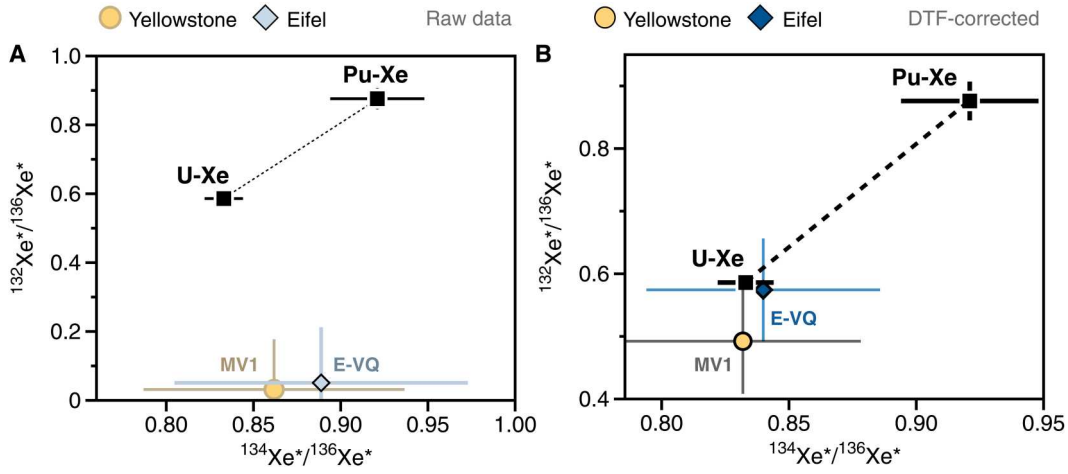


**Fig. 7. $^{132}Xe^*/^{136}Xe^*$ versus $^{134}Xe^*/^{136}Xe^*$ systematics of Yellowstone and Eifel samples with the highest mantle contributions reported in this study (i.e., MV1 and E-VQ, respectively), before and after DTF correction.** (**A** and **B**) The pure uranium (U-Xe) and plutonium (Pu-Xe) fissiogenic end-members (*17*) are shown as black squares. Once corrected for DTF, MV1 and E-VQ samples both appear most consistent with fissiogenic Xe isotopes deriving from uranium.

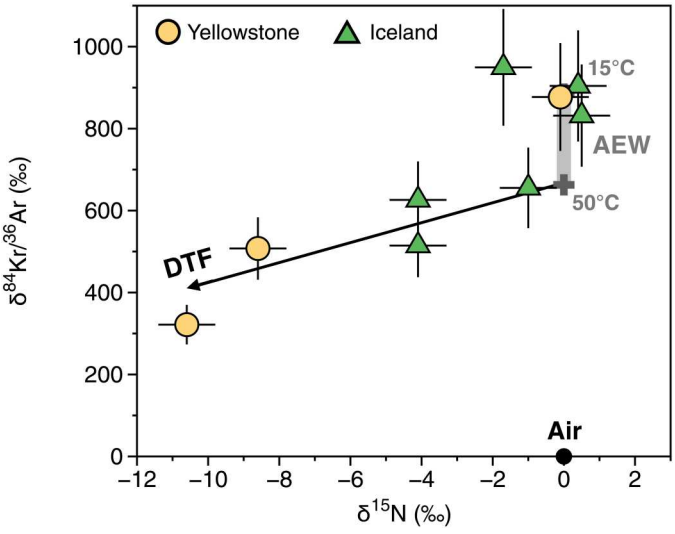


**Fig. 8. $\delta^{84}Kr/^{36}Ar$ versus $\delta^{15}N$ for Iceland and Yellowstone samples with air-like $\Delta_{30}$ values of 16‰ and higher.** (*37*) The observed trend implies that N loss causing $\delta^{15}N$ variations occurs together with preferential Kr and Xe losses relative to Ar. This is in contrast with predictions based on solubilities obtained in ideal conditions, where both Kr and Xe are expected to be more soluble than Ar. Previous studies therefore suggested that this may represent degassing of air-saturated water under extreme temperature and pressure conditions (*37*), where gas solubilities deviate considerably from a behavior governed by Henry's law (*60*). Here, we show that the observed trend is compatible with DTF of a gas phase that was stripped off a deep groundwater component with the elemental composition of AEW at ~50°C. This suggests that $\delta^{15}N$ of $N_2$, like noble gases, is affected by the same DTF processes that appear to be ubiquitous in volcanic gas systems worldwide (*43*).

To further test the hypothesis that DTF is a major cause of N isotope variations in volcanic gas samples, we measured the $\delta^{15}N$ composition of copper tube volcanic gas samples collected in Iceland and Yellowstone along with the Giggenbach bottles analyzed in this study (Fig. 2B) and tested whether a correlation could be found between the $\delta^{15}N$ of the copper tubes and the noble gas systematics of the corresponding Giggenbach bottles. This approach is, however, not ideal because, without knowledge of the $\Delta^{30}N$ composition of each sample, it is not possible to distinguish the relative effects of source contributions versus secondary processes, on the observed $\delta^{15}N$ variations (*37*). In addition, although there is no a priori reason to think that the compositions of the copper tube and Giggenbach bottle gas samples should be different from one another, as they sample the same volcanic gas emanation, there is no guarantee that these samples are actually identical. For example, Giggenbach samples contain volcanic gas that has been accumulated for several hours, and copper tube samples only provide access to the composition of the gas that was present in the system at the end of the sampling procedure (i.e., when the copper tube was closed following ample flushing). Because the temporal variability of volcanic gas emanations is not well constrained, we cannot exclude the possibility of significant compositional differences between copper tubes and corresponding Giggenbach bottle gas samples, however unlikely this may be. Figure S3 shows copper tube $\delta^{15}N$ variations as a function of the corresponding Giggenbach $\delta^{86}Kr/^{84}Kr$. Yellowstone and Iceland volcanic gas samples display lighter N isotope compositions and greater extents of DTF than Chilean samples, with a general trend of decreasing $\delta^{15}N$ with decreasing $\delta^{86}Kr/^{84}Kr$. This general trend appears consistent with the highly variable $\delta^{15}N$ of air-derived $N_2$ in volcanic systems worldwide (*37*, *40*, *41*) primarily arising from DTF. Further testing this hypothesis will, however, require coupling high-precision dynamic measurements of heavy noble gas isotopes and nitrogen isotopologues from volcanic gas samples collected in Giggenbach bottles.

DTF may affect many other volatile species than nitrogen and noble gases in volcanic systems. Predictions for steady-state isotope fractionation via DTF through $CO_2$ [with diffusion volumes of He and Ne equal to 2.67 and 5.98, respectively; (*31*, *32*)] indicate $^3He/^4He$ and $^{20}Ne/^{22}Ne$ fractionations of up to 143 and 16‰ $u^{-1}$, respectively. Therefore, starting from an atmosphere-like composition (i.e., $^3He/^4He = R_A$ and $^{20}Ne/^{22}Ne = 9.8$), DTF may produce $^3He/^4He$ and $^{20}Ne/^{22}Ne$ ratios of up to 1.14 $R_A$ and 10.1, respectively. While this isotopic effect appears small (but nonnegligible) for He, being comparable to the actual precision of typical mass spectrometers, the magnitude of Ne isotopic anomalies generated by DTF may be significant, representing up to ~11% of Ne isotope signals expected for a pure upper mantle source ($^{20}Ne/^{22}Ne$ ~ 12.5). Therefore, correction for DTF may be crucial for interpreting not only heavy noble gas isotope signals in volcanic systems but also nitrogen, neon, and potentially many other volatile species that are used to inform the composition of the solid Earth.

## Toward a physical model of subsurface fractionation

Correcting volatile isotope systematics for physical fractionation in the subsurface is required before any reliable interpretation of mantle-derived signals can be made. While the empirical correction developed in this study offers a promising avenue for correcting Xe isotopes for physical fractionation in the subsurface, in a consistent way across volcanic provinces worldwide, a contextualization of, and physical justification for, the occurrence of DTF in hydrothermal systems is required. One important observation is that volcanic gas samples with both air-like and AEW-like elemental ratios are associated with unfractionated isotopes, whereas intermediate elemental ratios show the largest extents of mass-dependent fractionation relative to the atmosphere (Fig. 2B). Samples with either air-like (i.e., $\delta^{84}Kr/^{36}Ar$ ~ 0‰) or AEW-like [i.e., $\delta^{84}Kr/^{36}Ar$ ~ 700 to 1000‰; assuming negligible contribution from the "salt effect" on noble gas solubilities (*44*)] noble gas elemental ratios show only limited isotopic deviation from the atmospheric isotope composition (Fig. 9). Given that the stripping of groundwater noble gases by $CO_2$ bubbles is known to induce extensive groundwater degassing causing the incorporation of AEW-like noble gases into the gas flow (*45*), the occurrence of an AEW-like component is not surprising. Conversely, the occurrence of unfractionated air in volcanic gas needs to be explained. The likelihood of air contamination during sampling is low, as $CO_2$ gas is systematically collected from surface water within an upside-down funnel, before the gas flow reaches the atmosphere (Fig. 3B). Submerging the exhaust tubing into a water container and checking for continuous gas flow through the system (i.e., constant bubbling rate at the exhaust) further provides a robust means to ensure that there is a net positive pressure of volcanic gas in the system and that no air is entering the Giggenbach bottle (and copper tubes; Fig. 3B). If the introduction of air-like noble gases into our sampling containers were to occur via leakage through a valve, then the sample gas should be highly fractionated, with

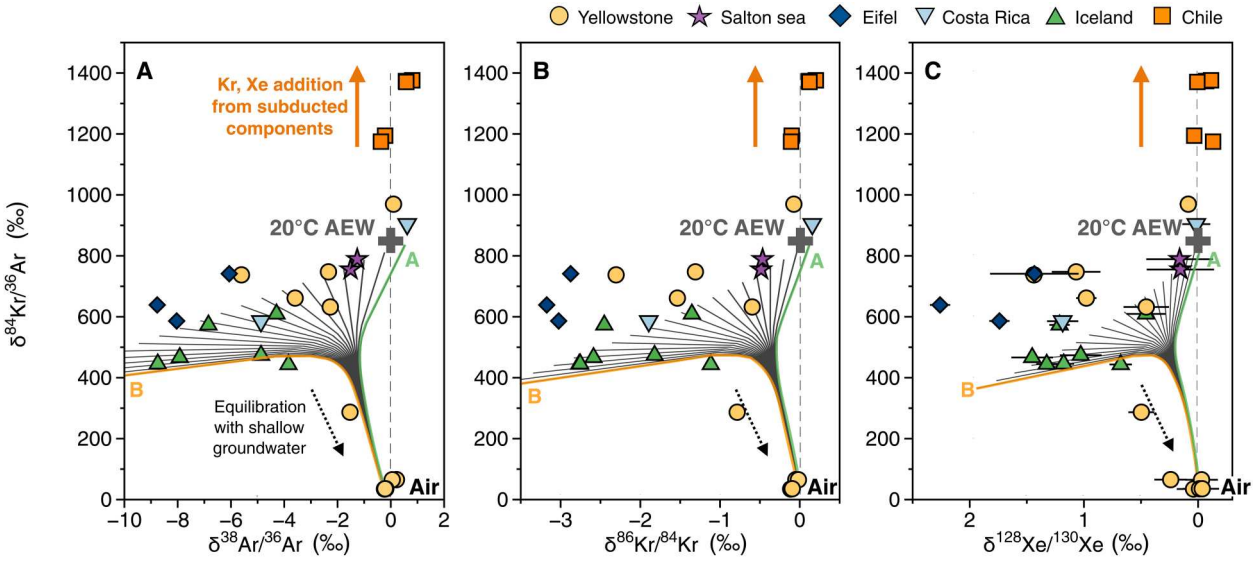


**Fig. 9. $\delta^{84}Kr/^{36}Ar$ versus $\delta^{38}Ar/^{36}Ar$, $\delta^{86}Kr/^{84}Kr$, and $\delta^{128}Xe/^{130}Xe$ isotope systematics and their comparison with predictions from the idealized model of subsurface fractionation.** (**A** to **C**) This model simulates the evolution of deep groundwater-derived noble gases due to progressive interaction with shallow groundwater (see MATLAB code; Supplementary Materials). Each separate line represents a different trajectory of equilibration between shallow groundwater and an initial gas phase representing deep groundwater-derived noble gases that have been variably fractionated because of DTF, depending on the advection/diffusion ratios [from pure advection by $CO_2$ without fractionation (green line, noted A) to extensive fractionation due to diffusion through $CO_2$ (orange line, noted B); fig. S8]. While this conceptual model readily explains elemental ratios varying between AEW (here shown for 20°C water) and air, without requiring mixing with unfractionated air during sampling, samples with $\delta^{84}Kr/^{36}Ar$ greater than AEW (e.g., Chile) likely require addition of extra Kr and Xe from the contribution of subduction-derived components, as suggested by carbon isotope systematics (fig. S2).

elemental ratios lower than air (i.e., negative $\delta^{84}Kr/^{36}Ar$, which is never observed). Here, the fact that only samples with intermediate elemental ratios between air and AEW are isotopically fractionated (Fig. 9) is an important indication that fractionation must be occurring in the subsurface, rather than during sample collection or processing. Last, we note that every single sample was rigorously leak checked once attached to the extraction system, before opening the Giggenbach bottle's valve for gas purification and analysis: The absence of detectable leakage at that stage is considered as good evidence that the samples did not suffer from any leakage during transport and storage.

All noble gas data reported here are consistent with quantitative degassing of deep groundwater into a large volume of subsurface $CO_2$, followed by variable extents of (i) horizontal diffusion of groundwater-degassed noble gases through $CO_2$ toward the center of an upwelling gas flow and (ii) near the surface, gas exchange with young (short residence time scale), air-equilibrated groundwater (Fig. 10). In this scenario, we consider a large, deep $CO_2$ gas reservoir containing mantle-derived noble gases, as well as AEW-like noble gases derived from extensive $CO_2$ stripping of deep groundwater. The extensive degassing of the deep groundwater reservoir is made possible by its characteristically long residence time scale. Because of the large $CO_2$ gas/water volume ratio in the deep subsurface, groundwater-derived noble gases are present in low abundances. They undergo lateral diffusion through quiescent $CO_2$ [and hence DTF; Fig. 3C] toward the upwelling plume of volcanic gas, where they are vigorously transported toward the surface by pure advection (Fig. 10). The extent of DTF through $CO_2$ (likely related to how far noble gases have to diffuse in order to reach the upwelling plume of $CO_2$) thus controls the degree of noble gas fractionation in the deep subsurface. Once the upwelling plume of $CO_2$ reaches shallow subsurface levels, it contains low concentrations of mantle and AEW-like noble gases that have been variably affected by DTF. If the plume of $CO_2$ reaches the surface without interacting with shallow groundwater, the composition of deep groundwater-derived noble gases (variably affected by DTF) will be preserved. However, if the plume of $CO_2$ starts equilibrating with shallow groundwater, then its composition will begin being overprinted by diffusive ingassing of shallow groundwater-derived noble gases, which induces fractionation of the elemental ratios due to the different diffusivities of Kr and Xe in water (Fig. 10).

In the proposed model, shallow groundwater is assumed to have a short residence time and is thus at equilibrium with air (i.e., with an AEW-like noble gas composition). Because the composition of noble gases acquired from complete equilibration of shallow groundwater equilibrated with an upwelling bubble of $CO_2$ gas is governed by solubility fractionation factors, the elemental and isotopic composition of groundwater-derived noble gases in the $CO_2$ plume will become close to unfractionated air as the $CO_2$ bubbles progressively reach equilibrium with shallow groundwater (Fig. 10). We propose here that the variable degrees of equilibration between the magmatic $CO_2$ (initially containing no AEW-like noble gases) and shallow groundwater readily account for the fact that noble gas elemental ratios in volcanic gases span the entire range of compositions between air and AEW (Fig. 2), without requiring mixing with air during sampling. Thus, the extent of gas interaction with atmosphere-derived noble gases in shallow groundwater ultimately controls the mantle fraction of total noble gases (with, e.g., the difference between the Xe isotopic spectra of E-VQ and E-SQ samples from Eifel primarily reflecting variable degrees of

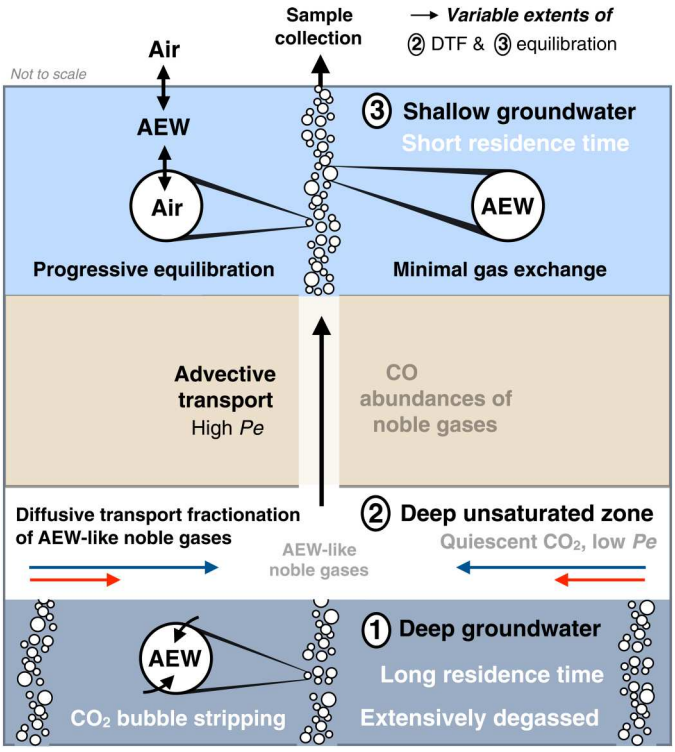


**Fig. 10. Schematic representation of our idealized model of subsurface fractionation, from deep to shallow groundwater levels.** The deep groundwater reservoir is considered to be extensively degassed as a result of protracted noble gas stripping by $CO_2$ bubbles. Depending on the advection/diffusion ratio [referred to as the Péclet number (*Pe*)], groundwater-derived noble gases in the deep unsaturated zone may then undergo variable extents of (i) DTF against $CO_2$ and (ii) advective transport toward the shallow groundwater level. Last, as the $CO_2$ plume accumulates shallow groundwater-derived noble gases, the gas phase gets closer to being in equilibrium with AEW. If it eventually reaches equilibrium, then its elemental and isotopic composition becomes indistinguishable from air. Intermediate stages of DTF and equilibration with shallow groundwater are required to explain the range of isotopic and elemental compositions observed in natural volcanic gas samples worldwide (Fig. 9).

"overprinting" during interaction with shallow groundwater; Fig. 6). This model predicts that (i) air-like elemental ratios will be accompanied by a lack of isotopic fractionation (with respect to air) due to extensive exchange with shallow groundwater, and (ii) AEW-like elemental ratios will also appear isotopically air-like (or slightly modified by weak solubility isotope effects) due to transport of deep, quantitatively degassed noble gases near the upwelling plume center, without extensive horizontal diffusion. The predicted lack of isotopic fractionation associated with both air-like and AEW-like (but not intermediate) elemental ratios is apparent in the data (Fig. 9). At last, this model also accounts for the observation of a wide range of isotopic fractionation among samples with similar, intermediate-type elemental ratios. While the most fractionated samples reflect DTF, the "least fractionated" samples would result from an initial (low abundance) ASW-like component that partially equilibrated with shallow groundwater, with the slight light isotope enrichment arising from the faster diffusion of lighter isotopes from shallow groundwater during diffusive degassing.

To more quantitatively explore this conceptual model, we built a numerical model that, for variable advection/diffusion ratios [referred to as the Péclet number (*Pe*)] of the deep groundwater-derived noble gas component, simulates the evolution of groundwater-derived noble gases due to progressive interaction with shallow groundwater (fig. S8). On Fig. 9, each separate line represents a different trajectory of equilibration between shallow groundwater and an initial gas phase representing deep groundwater-derived noble gases that have been variably fractionated because of DTF. The good agreement between model predictions and data (Fig. 9) suggests that the scenario of DTF proposed in this study (Fig. 10) satisfactorily captures the series of physical processes occurring within hydrothermal systems. In detail, several processes could represent additional (but likely minor) sources of noble gas isotope fractionation in the subsurface. The observation that the most extreme light isotope enrichments observed for noble gases and nitrogen in volcanic effusions worldwide do not extend pass the expectations for steady-state isotope fractionation is an indication that Rayleigh distillation is not happening to a significant extent during DTF, in line with the slow nature of diffusion processes in the deep unsaturated zone (i.e., long time scales). However, solubility-controlled noble gas isotope fractionation is one process that could enrich the gas phase in heavy isotopes relative to the water phase, by ~0.060 and ~0.025‰ $u^{-1}$ for Kr and Xe, respectively (*25*). In addition, gravitational settling in soil air may cause significant heavy noble gas isotope variations in natural gas systems, with depth-proportional heavy isotope enrichments (~0.004‰ $u^{-1}$ $m^{-1}$) across the unsaturated zone [i.e., above the water table; (*46*)]. Previous studies have shown that this heavy isotope enrichments can be recorded into the deep groundwater noble gas composition during equilibrium dissolution of soil air at the time of recharge (*46*, *47*). Hence, we cannot exclude the possibility that some of the deep groundwater components contain heavy Kr and Xe isotope enrichments inherited from gravitational settling in the unsaturated zone, at the time of their recharge. This could be the case for some of our samples from Chile and Costa Rica, which exhibit slight heavy Kr and Xe isotope enrichments relative to air (e.g., Fig. 2B). These samples also have $\delta^{84}Kr/^{36}Ar \geq$ AEW (Fig. 9), suggesting limited —if any—equilibration with shallow groundwater, in agreement with a preservation of deep groundwater-derived signals. The $\delta^{132}Xe/^{36}Ar$ and $\delta^{84}Kr/^{36}Ar$ values greater than AEW further point to a contribution from Xe- and Kr-rich components that, given the geological context of the samples (i.e., subduction zones), likely reflect a contribution from recycled organic materials and sediments (*12*). This is supported by the fact that Chilean samples display $\delta^{13}CO_2$ values below the mantle value (fig. S2) and positive $\delta^{15}N$ up to +4.17‰ (Campanario; fig. S3), potentially tracking a contribution from recycled organic sediments ($\delta^{13}C \sim -25$‰ and $\delta^{15}N \sim +6$‰) (*4*, *38*, *39*, *48*). Here, we cannot exclude the possibility that light $\delta^{13}CO_2$ values in the Southern Volcanic Zone (SVZ)—at least partly—reflect secondary processes associated with calcite precipitation in shallow hydrothermal systems (*7*, *27*). Likewise, we cannot exclude the possibility that some of the carbon and noble gases collected in Chilean volcanic emissions originate from organic sediments in the continental crust (rather than from recycling of slab materials). However, the fact that we only observe these light $\delta^{13}C$, heavy $\delta^{15}N$, and high $\delta^{132}Xe/^{36}Ar$-$\delta^{84}Kr/^{36}Ar$ values in the Chilean volcanic arc provides supporting evidence that heavy noble gas and carbon systematics can be

combined in future studies to document the fate of volatile elements in subduction zones.

Previous observations of significant heavy Kr isotope enrichments in magmatic $CO_2$ natural gases have been attributed to the occurrence of chondritic heavy noble gases (*9*, *16*). However, the extrapolation of these measured heavy Kr isotope enrichments toward potential cosmochemical end-members could be greatly affected by the widespread occurrence of DTF in these systems. A similar conclusion can be drawn for previously reported light Xe isotope enrichments, which have also been attributed to the occurrence of a chondritic signal (*9*, *15*–*17*) and yet could—at least in part—arise from DTF. Evaluating the extent to which the noble gas composition of a hydrothermal/volcanic gas sample has been affected by DTF is therefore warranted before any interpretation can be made regarding the cosmochemical origin of potential primordial signals in volcanic gases worldwide. Future DMS analyses of gas samples for which chondritic noble gas signals have been previously observed will dictate whether or not a complete reevaluation of their conclusions is warranted. If not, these DMS analyses will allow for a better-constrained insight into the origin and evolution of terrestrial volatiles than achieved today. At last, we note that the process of subsurface physical fractionation described here above is unlikely to affect the composition of volatiles trapped in volcanic rocks and minerals. Determining the composition of mantle-derived heavy noble gases from the analysis of volcanic rocks and minerals is, however, inherently challenging due to (i) the limited spatial distribution and availability of high-quality samples and (ii) the exceedingly low amounts of gas available for analysis. To achieve sufficient analytical precision, gas accumulation techniques have been used (*49*), but reanalyses of the same basaltic glass sample (e.g., popping rock 2∏D43) with different techniques have recently yielded inconsistent estimates of the relative contribution of Pu-Xe to total fissiogenic Xe in the upper mantle (*14*, *17*). Although there is a crucial need to understand the source(s) of these discrepancies, ongoing and future analytical developments in the analysis of noble gases trapped in basaltic glasses and melt inclusions represent a promising avenue for better determining the composition of mantle source reservoirs, providing complementary information to that provided by the DMS analysis of globally distributed hydrothermal systems.

In fine, DMS is a new analytical means of measuring volcanic noble gas isotopes. Because of its considerable improvement in analytical precision and accuracy over conventional techniques, it offers unprecedented insights into volcanic noble gas systematics and ultimately the origin and evolution of volatile elements on Earth. Here, we have shown that DTF through a $CO_2$ gas phase is the main process causing isotope fractionation of most volatile species (i.e., at least nitrogen and noble gases) in the subsurface. Light Xe isotope excesses (i.e., positive $\delta^{128}Xe/^{130}Xe$ values) of up to ~1‰ $u^{-1}$ in volcanic gases may thus—at least partially and, in most cases, fully—reflect physical isotope fractionation of groundwater-derived noble gases, rather than primordial signals. After correction for DTF, Xe isotope spectra generated by DMS can be used to disentangle crustal and mantle-derived contributions in a wide range of samples previously out of reach to traditional measurement techniques. Furthermore, this technique has the potential to provide crucial insight into the Xe isotope composition of deep mantle sources (e.g., $^{129}Xe^*/^{136}Xe^*$, deconvolution of $^{136}Xe_{Pu}$ and $^{136}Xe_U$ signals), even for samples with only a few percent contribution of mantle Xe. If applied to more regions globally, volcanic noble gas analysis by DMS has the potential to markedly change our understanding of mantle source heterogeneities and terrestrial volatile evolution.

## MATERIALS AND METHODS

### Sample collection

In this study, "dry" (volcanic) gas samples were collected from hydrothermal systems in Chile [Baño Morales and Campanario springs, SVZ (*27*)], Iceland [Krýsuvík and Reykjanes (Gunnuhver) hot springs (*40*)], Germany [E-VQ and E-SQ wells in Eifel (*17*)], Costa Rica [Praxair well #17 and Poás Volcano (*7*)], and United States [across the Yellowstone National Park (Washbun Spring, Forrest Spring, Crater Hills, Mud Volcano) (*33*) and Salton Sea Geothermal System (Davis-Schrimpf mud volcanoes) (*50*)]. At each sampling location, we collected copper tubes and "Giggenbach" bottles. The latter collection method facilitates the collection of up to five orders of magnitude larger samples than traditional methods when gases are rich in reactive and condensable species [such as $CO_2$, $H_2O$, $SO_2$, and $H_2S$ (*17*)].

### Noble gas measurements by DMS (Seltzer Lab, WHOI)

All Giggenbach samples were analyzed using a recently developed technique for DMS analysis (*21*) in the Seltzer Lab at WHOI. In the past, two major challenges have precluded DMS measurement of noble gas isotopes in volcanic gas samples. The first is sample size, and the second concerns the unknown elemental ratios of volcanic gas samples. For dual-inlet DMS analysis, one must have sufficient pressure to ensure viscous flow, and be able to balance the total pressure between the bellows containing the sample gas and those containing a reference gas. To solve the first challenge, large volumes (hundreds of liters) of volcanic gas were concentrated within evacuated 1.5-liter Giggenbach bottles by using a caustic (NaOH) solution that efficiently traps $CO_2$ (and other acidic gases) and leaves the headspace volume of the bottle to be filled with nonreactive species, such as noble gases (*17*, *51*). This technique allows accumulation of ≥1 $cm^3$ at standard temperature and pressure (STP) of $^{40}Ar$ gas, which is sufficient to ensure viscous flow during noble gas analysis by DMS. With respect to the second challenge, Kr/Ar and Xe/Ar of a volcanic gas can vary widely, but the new analytical technique (*21*) takes advantage of the fact that >99.8% of all the heavy noble gases in volcanic gas is $^{40}Ar$. By matching $^{40}Ar$ ion beam intensities between sample and reference gases, this technique ensures that the total pressure during analysis is balanced between sample and reference gases; in other words, Kr and Xe isotopes can be analyzed with an assurance of balanced pressure, independent of Kr/Ar and Xe/Ar. Small, but important, corrections for instrumental nonlinearity and matrix effects are also a key advance of the new technique (*21*).

### Carbon isotope measurements (Subhas Lab, WHOI)

Giggenbach solutions ($CO_2$-saturated sodium hydroxide) were stored in sealed high-density polyethylene bottles until analysis. Because of a spectroscopic interference between sulfide and carbon dioxide, samples were treated to quantitatively oxidize sulfide to sulfate (*52*). About 5 ml of solution was transferred via pipette to a 25-ml volumetric flask. Sulfides were oxidized to sulfate by adding hydrogen peroxide [30 wt %; Acros Organics lot

B0543448A] in 50 μl of increments until bubbling was observed. About 0.1 ml of the resulting solution was added via syringe to an evacuated 12-ml exetainer vial (Labco 938W). Samples were diluted with milliQ water and acidified using 10% phosphoric acid (Thermo Fisher Scientific, lot 200228). The resulting $CO_2$ was analyzed using a Picarro G-2131i cavity ringdown spectrometer connected to an AutoMate-Liaison prep device. The resulting isotopic and concentration data were standardized against both in-house and International Atomic Energy Agency standard materials analyzed during each analytical session (*53*).

### Nitrogen and helium isotope measurements (Barry Lab, WHOI)

The He and nitrogen isotope compositions of copper tube volcanic gas samples collected in this study were measured separately using the Noblesse Nu mass spectrometer in the Barry Lab at WHOI. For He isotope measurements (*27*), copper tube samples were connected to a noble gas extraction line using an O-ring connection, and ~5 $cm^3$ of gas was expanded into the cleanup line. The pressure was measured using a capacitance manometer, and then a small aliquot of gas was expanded into the cleanup portion of the line. Reactive gases were chemically removed by exposing gases to a titanium sponge held at 650°C. The titanium sponge was then cooled for 10 min to room temperature to getter hydrogen before gases were expanded to a dual hot (SAES ST707) and cold (SAES ST707) getter system, held at 250°C and room temperature, respectively. Another small aliquot of gas was then segregated for preliminary analysis on a quadrupole mass spectrometer. Noble gases were separated using a series of cryogenic traps, cooled using helium compressors. The heavy noble gases (Ar-Kr-Xe) were adsorbed at 30 K onto a nude stainless steel trap, and He and Ne were adsorbed at 10 K on a charcoal trap. The temperature of the charcoal trap was then raised to 30 K, releasing only He, which was then inlet into the Noblesse mass spectrometer. Following He abundance and isotope determination, the temperature on the charcoal cryogenic trap was raised to 80 K for 15 min to release Ne, which was inlet into the Noblesse mass spectrometer. Following Ne measurement, the nude and charcoal cryogenic traps were raised to 300 K for cleanup. Air standards were analyzed daily from an air cylinder collected on the roof of the Clark Laboratory building on WHOI's Quissett campus on 15 September 2020. Air standards are fully automated and run overnight, following sample analysis during the day. Air standards were run for He and Ne using an identical method to the one employed for samples. Air standards were measured over a concentration range, which spanned two orders of magnitude, to account for any nonlinearity of the system. Full procedural blanks were run weekly; average (mean) $^4$He blanks and $^{20}$Ne blanks were less than 5% of the sample size. For nitrogen isotope measurements, copper tube samples were connected to a separate extraction line using an O-ring connection, and ~5 $cm^3$ of gas was expanded into the vacuum gas purification line, before following the purification procedure described by (*54*). The gas fraction dedicated to N isotope measurements was exposed to a copper oxide (CuO) finger (at 850°C) in the presence of a platinum foil catalyst (at 1000°C), which promotes oxidation of carbonaceous (CO; $C_2H_4$) and nitrogenous (NO) species to $CO_2$ and $NO_2$, while any residual hydrogen and sulfur were oxidized to $H_2O$ and $SO_2$, respectively. All condensable species produced at this stage are adsorbed onto a Pyrex cold finger held at liquid nitrogen temperature. Oxygen was then reabsorbed back onto the CuO finger at a lower temperature (≤600°C) before the oxidized gas was inlet into the Noblesse mass spectrometer. During N isotope analysis, we simultaneously measure mass-to-charge ratio ($m/z$) = 28 and 29. In total, 20 data collection cycles are run per sample. Background levels are monitored between sample measurements to apply a background subtraction to all data. The nitrogen isotope ratio is calculated by extrapolating the data back to time zero (i.e., time of inlet into the mass spectrometer) using a linear fit. A CO correction is made by directly measuring CO at $m/z$ 28 and then applying a correction to the 28 and 29 peaks. This correction assumes that the CO contribution at mass 29 is 1.09% of the contribution at mass 28, based on the abundance ratio of $^{13}$C to $^{12}$C in air (*55*). The automatization of standard measurements allows a significant number of $N_2$ standards to be measured (about 50 analyses per day, on average), thus enabling precise characterization of the $N_2$ standard's composition, as well as quantification of (and correction for) linearity effects in the mass spectrometer.

### Modeling of noble gas degassing, transport, and interactions with groundwater

This idealized model considers the evolution of Ar, Kr, and Xe isotopes in a parcel $CO_2$-rich gas as it (a) is fractionated at depth in the gas phase by diffusion against $CO_2$ and subsequently (b) inherits Ar, Kr, and Xe through diffusive exchange with shallow groundwater before arriving at the surface, where it is sampled. At depth (stage a), we initially consider a $CO_2$-dominated gas phase that has quantitatively stripped (i.e., fully degassed) a deep old groundwater reservoir of its noble gases. For the (nonunique) example considered in this paper (Fig. 9), we consider an initial amount, $N_0$ (mol), of (nonradiogenic, nonradioactive) Ar in the $CO_2$ gas phase that is diluted from the atmosphere by a factor ω. The model tracks the evolution of a parcel of gas of volume, $V$ ($L$), as it ascends and interacts with shallow groundwater. The initial noble gas content of the deep source before ascending consists of degassed groundwater (that resembles AEW), modified by gas-phase fractionation against $CO_2$, based on an advection-diffusion ratio γ. We prescribe the initial $^{36}$Ar content ($N_{0,36Ar}$) before ascension as

$$N_{0,36Ar} = \frac{\chi_{atm,36Ar}}{M\omega} \tag{4}$$

where $\chi_{atm,36Ar}$ is the mole fraction of $^{36}$Ar in the atmosphere ($3.1 \times 10^{-5}$) and $M$ is the molar volume of Ar (22.39 liters). For a range of advection-diffusion ratios between 0 and 1, we then prescribe corresponding initial (deep) contents, $N_{0,i}$, of other noble gas isotopes, $i$ (where $i$ = $^{38}$Ar, $^{86}$Kr, $^{84}$Kr, $^{82}$Kr, $^{128}$Xe, or $^{130}$Xe), as

$$N_{0,i} = (1-\gamma)\frac{C_{ASW,i}}{C_{ASW,36Ar}} N_{0,36Ar} + \gamma \frac{C_{ASW,i}}{C_{ASW,36Ar}} N_{0,36Ar} \frac{D_{BD-CO2,i}}{D_{BD-CO2,36Ar}} \tag{5}$$

where $C_{ASW,i}$ (M) is the concentration of isotope $i$ in fresh water at solubility equilibrium at a prescribed recharge temperature $T$ (°C) according to (*25*, *56*) and $D_{BD-CO2,i}$ is the binary diffusivity ratio of isotope $i$ against $CO_2$ calculated using the method of (*30*), as presented in (*31*).

Next, as a parcel of $CO_2$-rich gas with diluted ASW-like or diffusively fractionated noble gas content ascends, it diffusively

exchanges gas (stage b), with shallow groundwater assumed to have an ASW-like composition at recharge temperature $T$. Our model considers the evolution of noble gas content in the parcel of gas as it progressively equilibrates with shallow groundwater (of equal volume $V$ to the gas phase considered, for simplicity). In this idealized model, we simply assume a diffusive length scale, $L$ (m), of 0.1 m for gas exchange with shallow groundwater, and we adopt a piston velocity, $k$ (m day$^{-1}$), for $^{36}$Ar of 1 m day$^{-1}$. Because of the vigorous bubbling observed in geothermal systems, we assume a Schmidt number exponent of −1/2 for a turbulent bubble-water interface (*57*), and we adopt the Ar, Kr, and Xe isotopic kinetic fractionation factors, $\alpha_{kin}$, of (*25*) and the diffusivities, $D$ (m$^2$ s$^{-1}$), of Kr and Xe (and assumed diffusivity of Ar) reported by (*58*), as compiled in the MATLAB script "gas_diffusion" (credit: R. Hamme). Note that we use the linear mass-fractionation relationships reported by (*25*) to infer the kinetic fractionation factor for the specific Ar, Kr, and Xe isotope ratios of interest in this study. With these assumptions, we calculate isotope-specific piston velocities, $k_i$, for bubble-water gas exchange in the following way for Ar isotopes

$$k_i = k_{36\mathrm{Ar}}\alpha_{\mathrm{kin}(i-36\mathrm{Ar})} \tag{6}$$

For Kr isotopes

$$k_i = k_{36\mathrm{Ar}}\left(\frac{D_{\mathrm{Kr}}}{D_{\mathrm{Ar}}}\right)^{1/2}\alpha_{\mathrm{kin}(i-84\mathrm{Kr})} \tag{7}$$

For Xe isotopes

$$k_i = k_{36\mathrm{Ar}}\left(\frac{D_{\mathrm{Xe}}}{D_{\mathrm{Ar}}}\right)^{1/2}\alpha_{\mathrm{kin}(i-130\mathrm{Xe})} \tag{8}$$

Last, using these isotope-specific piston velocities, we simulate the impact of bubble-water gas exchange on bubble composition by numerically integrating the one-dimensional diffusion equation. The content of isotope $i$ in a bubble at time $t$ is given by the following

$$N_i(t) = N_i(t-dt) + \frac{k_i}{L}\left(C_{\mathrm{ASW},i} - \frac{N_{i(t)}}{VH_i}\right)dt \tag{9}$$

where $H_i$ refers to the dimensionless Henry coefficient (i.e., $C_{gas}/C_{dissolved}$ at equilibrium in fresh water at temperature $T$) for isotope $i$ based on (*25*, *56*). Deviations from the atmosphere, δ (‰), are then simply calculated for any two isotopes, $a$ and $b$ with atmospheric ratio $(a/b)_{atm}$, at any time $t$

$$\delta(t) = \left[\frac{\frac{N_a(t)}{N_b(t)}}{\left(\frac{a}{b}\right)_{\mathrm{atm}}} - 1\right]10^3 \tag{10}$$

These equations are implemented in the accompanying MATLAB script "subsurface_fractionation_model.m" and its associated scripts. Figure 9 shows idealized model trajectories assuming ω = 100, $T$ = 20°C, $L$ = 0.1 m, $k_{36}$ = 1 m d$^{-1}$ integrated with $dt$ = 0.1 day, for the time-dependent evolution of bubble composition with initial (deep/stage a) compositions that range from the purely advective (unfractionated ASW) to purely diffusive (heavily fractionated) end-members.

## Supplementary Materials

**This PDF file includes:**
Figs. S1 to S8
References

**Other Supplementary Material for this manuscript includes the following:**
Data S1

## REFERENCES AND NOTES


1. M. W. Broadley, D. V. Bekaert, L. Piani, E. Füri, B. Marty, Origin of life-forming volatile elements in the inner Solar System. *Nature* **611**, 245–255 (2022).
2. D. C. Rubie, S. A. Jacobson, A. Morbidelli, D. P. O'Brien, E. D. Young, J. de Vries, F. Nimmo, H. Palme, D. J. Frost, Accretion and differentiation of the terrestrial planets with implications for the compositions of early-formed Solar System bodies and accretion of water. *Icarus* **248**, 89–108 (2015).
3. C. M. O. D. Alexander, The origin of inner solar system water. *Philos. Trans. R. Soc. A Math. Phys. Eng. Sci.* **375**, 20150384 (2017).
4. D. V. Bekaert, S. J. Turner, M. W. Broadley, J. D. Barnes, S. A. Halldórsson, J. Labidi, J. Wade, K. J. Walowski, P. H. Barry, Subduction-driven volatile recycling: A global mass balance. *Annu. Rev. Earth Planet. Sci.* **49**, 37–70 (2021).
5. B. Marty, The origins and concentrations of water, carbon, nitrogen and noble gases on Earth. *Earth Planet. Sci. Lett.* **313–314**, 56–66 (2012).
6. A. N. Halliday, The origins of volatiles in the terrestrial planets. *Geochim. Cosmochim. Acta* **105**, 146–171 (2013).
7. P. H. Barry, J. M. de Moor, D. Giovannelli, M. Schrenk, D. R. Hummer, T. Lopez, C. A. Pratt, Y. A. Segura, A. Battaglia, P. Beaudry, G. Bini, M. Cascante, G. d'Errico, M. di Carlo, D. Fattorini, K. Fullerton, E. Gazel, G. González, S. A. Halldórsson, K. Iacovino, J. T. Kulongoski, E. Manini, M. Martínez, H. Miller, M. Nakagawa, S. Ono, S. Patwardhan, C. J. Ramírez, F. Regoli, F. Smedile, S. Turner, C. Vetriani, M. Yücel, C. J. Ballentine, T. P. Fischer, D. R. Hilton, K. G. Lloyd, Forearc carbon sink reduces long-term volatile recycling into the mantle. *Nature* **568**, 487–492 (2019).
8. S. Mukhopadhyay, R. Parai, Noble gases: A record of Earth's evolution and mantle dynamics. *Annu. Rev. Earth Planet. Sci.* **47**, 389–419 (2019).
9. M. W. Broadley, P. H. Barry, D. V. Bekaert, D. J. Byrne, A. Caracausi, C. J. Ballentine, B. Marty, Identification of chondritic krypton and xenon in Yellowstone gases and the timing of terrestrial volatile accretion. *Proc. Natl. Acad. Sci. U.S.A.* **117**, 13997–14004 (2020).
10. S. Péron, S. Mukhopadhyay, M. D. Kurz, D. W. Graham, Deep-mantle krypton reveals Earth's early accretion of carbonaceous matter. *Nature* **600**, 462–467 (2021).
11. I. Tolstikhin, B. Marty, D. Porcelli, A. Hofmann, Evolution of volatile species in the earth's mantle: A view from xenology. *Geochim. Cosmochim. Acta* **136**, 229–246 (2014).
12. G. Holland, C. J. Ballentine, Seawater subduction controls the heavy noble gas composition of the mantle. *Nature* **441**, 186–191 (2006).
13. R. Parai, S. Mukhopadhyay, Xenon isotopic constraints on the history of volatile recycling into the mantle. *Nature* **560**, 223–227 (2018).
14. R. Parai, S. Mukhopadhyay, Heavy noble gas signatures of the North Atlantic Popping Rock 2ΠD43: Implications for mantle noble gas heterogeneity. *Geochim. Cosmochim. Acta* **294**, 89–105 (2021).
15. M. W. Caffee, G. B. Hudson, C. Velsko, G. R. Huss, E. C. Alexander Jr., A. R. Chivas, Primordial noble gases from Earth's mantle: Identification of a primitive volatile component. *Science* **285**, 2115–2118 (1999).
16. G. Holland, M. Cassidy, C. Ballentine, Meteorite Kr in Earth's mantle suggests a late accretionary source for the atmosphere. *Science* **326**, 1522–1525 (2009).
17. D. V. Bekaert, M. W. Broadley, A. Caracausi, B. Marty, Novel insights into the degassing history of Earth's mantle from high precision noble gas analysis of magmatic gas. *Earth Planet. Sci. Lett.* **525**, 115766 (2019).
18. K. Nagao, N. Takaoka, O. Matsubayashi, Isotopic anomalies of rare gases in the Nigorikawa geothermal area, Hokkaido, Japan. *Earth Planet. Sci. Lett.* **44**, 82–90 (1979).
19. K. Nagao, N. Takaoka, O. Matsubayashi, Rare gas isotopic compositions in natural gases of Japan. *Earth Planet. Sci. Lett.* **53**, 175–188 (1981).
20. B. Marty, On the noble gas isotopic fractionation in naturally occurring gases. *Geochem. J.* **18**, 157–162 (1984).
21. A. M. Seltzer, D. V. Bekaert, A unified method for measuring noble gas isotope ratios in air, water, and volcanic gases via dynamic mass spectrometry. *Int. J. Mass Spectrom.* **478**, 116873 (2022).

22. C. R. McKinney, J. M. McCrea, S. Epstein, H. A. Allen, H. C. Urey, Improvements in mass spectrometers for the measurement of small differences in isotope abundance ratios. *Rev. Sci. Instrum.* **21**, 724–730 (1950).
23. K. E. Tempest, S. Emerson, Kinetic isotopic fractionation of argon and neon during air – water gas transfer. *Mar. Chem.* **153**, 39–47 (2013).
24. L. Tyroller, M. S. Brennwald, H. Busemann, C. Maden, H. Baur, R. Kipfer, Negligible fractionation of Kr and Xe isotopes by molecular diffusion in water. *Earth Planet. Sci. Lett.* **492**, 73–78 (2018).
25. A. M. Seltzer, J. Ng, J. P. Severinghaus, Precise determination of Ar, Kr and Xe isotopic fractionation due to diffusion and dissolution in fresh water. *Earth Planet. Sci. Lett.* **514**, 156–165 (2019).
26. J. P. Severinghaus, M. L. Bender, R. F. Keeling, W. S. Broecker, Fractionation of soil gases by diffusion of water vapor, gravitational settling, and thermal diffusion. *Geochim. Cosmochim. Acta* **60**, 1005–1018 (1996).
27. P. H. Barry, J. M. De Moor, A. Chiodi, F. Aguilera, M. R. Hudak, D. V. Bekaert, S. J. Turner, J. Curtice, A. M. Seltzer, G. L. Jessen, E. Osses, J. M. Blamey, M. J. Amenábar, M. Selci, M. Cascone, A. Bastianoni, M. Nakagawa, R. Filipovich, E. Bustos, M. O. Schrenk, J. Buongiorno, C. J. Ramírez, T. J. Rogers, K. G. Lloyd, D. Giovannelli, The helium and carbon isotope characteristics of the andean convergent margin. *Front. Earth Sci.* **10**, 897267 (2022).
28. A. M. Seltzer, J. A. Krantz, J. Ng, W. R. Danskin, D. V. Bekaert, P. H. Barry, D. L. Kimbrough, J. T. Kulongoski, J. P. Severinghaus, The triple argon isotope composition of groundwater on ten-thousand-year timescales. *Chem. Geol.* **583**, 120458 (2021).
29. M. L. Bender, B. Barnett, G. Dreyfus, J. Jouzel, D. Porcelli, The contemporary degassing rate of 40Ar from the solid Earth. *Proc. Natl. Acad. Sci. U.S.A.* **105**, 8232–8237 (2008).
30. E. N. Fuller, P. D. Schettler, J. C. Giddings, A new method for prediction of binary gas-phase diffusion coefficients. *Ind. Eng. Chem.* **58**, 18–27 (1966).
31. R. C. Reid, J. M. Prausnitz, T. K. Sherwood, *The Properties of Gases and Liquids* (McGraw-Hill Book Company, 1977).
32. W. Gu, P. Cheng, M. Tang, Compilation and evaluation of gas phase diffusion coefficients of halogenated organic compounds. *R. Soc. Open Sci.* **5**, 171936 (2018).
33. J. B. Lowenstern, W. C. Evans, D. Bergfeld, A. G. Hunt, Prodigious degassing of a billion years of accumulated radiogenic helium at Yellowstone. *Nature* **506**, 355–358 (2014).
34. R. O. Pepin, D. Porcelli, Xenon isotope systematics, giant impacts, and mantle degassing on the early Earth. *Earth Planet. Sci. Lett.* **250**, 470–485 (2006).
35. S. Mukhopadhyay, Early differentiation and volatile accretion recorded in deep-mantle neon and xenon. *Nature* **486**, 101–104 (2012).
36. R. Parai, S. Mukhopadhyay, J. M. Tucker, M. K. Pető, The emerging portrait of an ancient, heterogeneous and continuously evolving mantle plume source. *Lithos* **346**–**347**, 105153 (2019).
37. J. Labidi, P. H. Barry, D. V. Bekaert, M. W. Broadley, B. Marty, T. Giunta, O. Warr, B. Sherwood Lollar, T. P. Fischer, G. Avice, A. Caracausi, C. J. Ballentine, S. A. Halldórsson, A. Stefánsson, M. D. Kurz, I. E. Kohl, E. D. Young, Hydrothermal 15N15N abundances constrain the origins of mantle nitrogen. *Nature* **580**, 367–371 (2020).
38. B. Marty, N. Dauphas, The nitrogen record of crust-mantle interaction and mantle convection from Archean to present. *Earth Planet. Sci. Lett.* **206**, 397–410 (2003).
39. P. Cartigny, B. Marty, Nitrogen isotopes and mantle geodynamics: The emergence of life and the atmosphere-crust-mantle connection. *Elements* **9**, 359–366 (2013).
40. A. Stefánsson, D. R. Hilton, Á. E. Sveinbjörnsdóttir, P. Torssander, J. Heinemeier, J. D. Barnes, S. Ono, S. A. Halldórsson, J. Fiebig, S. Arnórsson, Isotope systematics of Icelandic thermal fluids. *J. Volcanol. Geotherm. Res.* **337**, 146–164 (2017).
41. B. Marty, E. Gunnlaugsson, A. Jambon, N. Oskarsson, M. Ozima, F. Pineau, P. Torssander, Gas geochemistry of geothermal fluids, the Hengill area, southwest rift zone of Iceland. *Chem. Geol.* **91**, 207–225 (1991).
42. L. Li, P. Cartigny, M. Ader, Kinetic nitrogen isotope fractionation associated with thermal decomposition of NH3: Experimental results and potential applications to trace the origin of N2 in natural gas and hydrothermal systems. *Geochim. Cosmochim. Acta* **73**, 6282–6297 (2009).
43. J. Labidi, E. D. Young, The origin and dynamics of nitrogen in the Earth's mantle constrained by $^{15}N^{15}N$ in hydrothermal gases. *Chem. Geol.* **591**, 120709 (2022).
44. S. P. Smith, B. M. Kennedy, The solubility of noble gases in water and in NaCl brine. *Geochim. Cosmochim. Acta* **47(3)**, 503–515 (1983).
45. S. M. V. Gilfillan, C. J. Ballentine, G. Holland, D. Blagburn, B. S. Lollar, S. Stevens, M. Schoell, M. Cassidy, The noble gas geochemistry of natural CO2 gas reservoirs from the Colorado Plateau and Rocky Mountain provinces, USA. *Geochim. Cosmochim. Acta* **72**, 1174–1198 (2008).
46. A. M. Seltzer, J. P. Severinghaus, B. J. Andraski, D. A. Stonestrom, Steady state fractionation of heavy noble gas isotopes in a deep unsaturated zone. *Water Resour. Res.* **53**, 2716–2732 (2017).
47. A. M. Seltzer, J. Ng, W. R. Danskin, J. T. Kulongoski, R. S. Gannon, M. Stute, J. P. Severinghaus, Deglacial water-table decline in Southern California recorded by noble gas isotopes. *Nat. Commun.* **10**, 5739 (2019).
48. Y. Sano, B. Marty, Origin of carbon in fumarolic gas from island arcs. *Chem. Geol.* **119**, 265–274 (1995).
49. S. Péron, M. Moreira, Onset of volatile recycling into the mantle determined by xenon anomalies. *Geochem. Perspect. Lett.* **9**, 21–25 (2018).
50. A. Mazzini, H. Svensen, G. Etiope, N. Onderdonk, D. Banks, Fluid origin, gas fluxes and plumbing system in the sediment-hosted Salton Sea Geothermal System (California, USA). *J. Volcanol. Geotherm. Res.* **205**, 67–83 (2011).
51. W. F. Giggenbach, A simple method for the collection and analysis of volcanic gas samples. *Bull. Volcanol.* **39**, 132–145 (1975).
52. K. Malowany, J. Stix, A. Van Pelt, G. Lucic, $H_2S$ interference on $CO_2$ isotopic measurements using a Picarro G1101-i cavity ring-down spectrometer. *Atmos. Meas. Tech.* **8**, 4075–4082 (2015).
53. A. V. Subhas, D. C. McCorkle, A. Quizon, A. P. McNichol, M. H. Long, Selective preservation of coccolith calcite in Ontong-Java Plateau sediments. *Paleoceanogr. Paleoclimatol.* **34**, 2141–2157 (2019).
54. P. H. Barry, D. R. Hilton, S. A. Halldórsson, D. Hahm, K. Marti, High precision nitrogen isotope measurements in oceanic basalts using a static triple collection noble gas mass spectrometer. *Geochem. Geophys. Geosyst.* **13**, Q01019 (2012).
55. H. Graven, R. F. Keeling, J. Rogelj, Changes to carbon isotopes in atmospheric $CO_2$ over the industrial era and into the future. *Global Biogeochem. Cycles* **34**, e2019GB006170 (2020).
56. W. J. Jenkins, D. E. Lott III, K. L. Cahill, A determination of atmospheric helium, neon, argon, krypton, and xenon solubility concentrations in water and seawater. *Mar. Chem.* **211**, 94–107 (2019).
57. B. Jähne, W. Huber, A. Dutzi, T. Wais, J. Ilmberger, in *Gas Transfer at Water Surfaces* (Springer Netherlands, 1984), pp. 303–309.
58. B. Jähne, G. Heinz, W. Dietrich, Measurement of the diffusion coefficients of sparingly soluble gases in water. *J. Geophys. Res. Oceans* **92**, 10767–10776 (1987).
59. D. York, N. M. Evensen, M. López Martínez, J. De Basabe Delgado, Unified equations for the slope, intercept, and standard errors of the best straight line. *Am. J. Phys.* **72**, 367–375 (2004).
60. O. Warr, C. A. Rochelle, A. Masters, C. J. Ballentine, Determining noble gas partitioning within a CO2-H2O system at elevated temperatures and pressures. *Geochim. Cosmochim. Acta* **159**, 112–125 (2015).
61. C. J. Ballentine, P. G. Burnard, Production, release and transport of noble gases in the continental crust. *Rev. Mineral. Geochem.* **47**, 481–538 (2002).


**Acknowledgments:** We thank the two anonymous reviewers for their very constructive suggestions that improved the quality and clarity of our manuscript. **Funding:** This study was funded by National Science Foundation (NSF) grant DEB-2132774 and Simons Foundation grant 404586 to K.G.L., NSF grant CH-2151120 to P.H.B. and A.M.S., NSF grant OCE-2122427 to A.M.S., Agence Nationale de la Recherche grant ANR-22-CPJ2-0005-01 to D.V.B., and European Research Council grant 695618 to B.M. D.G. was supported by funding from the European Research Council (ERC) under the European Union's Horizon 2020 research and innovation program Grant Agreement No. 948972—COEVOLVE—ERC-2020-STG. **Author contributions:** D.V.B., A.M.S., and P.H.B. designed the project. D.V.B., P.H.B., M.W.B., D.J.B., B.M., C.J.R., J.M.d.M., A.R., and S.A.H. contributed to the sampling. A.M.S. and D.V.B. carried out the noble gas analyses by DMS. D.V.B., M.R.H., and P.H.B. carried out the nitrogen isotope analyses. A.V.S. carried out the carbon isotope analyses. A.M.S. wrote the MATLAB code. D.V.B. wrote the initial version of the manuscript. All coauthors commented on the different versions of the paper, and all authors approved the final version. **Competing interests:** The authors declare that they have no competing interests. **Data and materials availability:** All data needed to evaluate the conclusions in the paper are present in the paper and/or the Supplementary Materials.

Submitted 12 December 2022
Accepted 16 March 2023
Published 14 April 2023
10.1126/sciadv.adg2566